U-Pb geochronology of the Tsineng dyke swarm and paleomagnetism of the Hartley Basalt Formation, South Africa – evidence for two separate magmatic events at 1.93 – 1.92 and 1.88 – 1.84 Ga in the Kalahari craton

Farnaz Alebouyeh Semami

Dissertations in Geology at Lund University,
Master's thesis, no 416
(45 hp/ECTS credits)

Department of Geology
Lund University
2014

U-Pb geochronology of the Tsineng dyke swarm and paleomagnetism of the Hartley Basalt Formation, South Africa – evidence for two separate magmatic events at 1.93 – 1.92 and 1.88 – 1.84 Ga in the Kalahari craton

Master's thesis

Farnaz Alebouyeh Semami

Department of Geology
Lund University
2014

Contents

Cover Picture: Uppermost layers of Hartley Basalt Formation. Photo by: Michiel De Kock

U-Pb geochronology of the Tsineng dyke swarm and paleomagnetism of the Hartley Basalt Formation, South Africa – evidence for two separate magmatic events at 1.93 – 1.92 and 1.88 – 1.84 Ga in the Kalahari craton

FARNAZ ALEBOUYEH SEMAMI

Alebouyeh Semami, F., 2014: U-Pb geochronology of the Tsineng dyke swarm and paleomagnetism of the Hartley Basalt Formation, South Africa – evidence for two separate magmatic events at 1.93 – 1.92 and 1.88 – 1.84 Ga in the Kalahari craton. *Dissertations in Geology at Lund University*, No. 416, 30 pp. 45 hp (45 ECTS credits).

Abstract: Robust geochronology and well-constrained paleopoles are the main tools for paleogeographic reconstructions. Through the completion of so called barcode diagrams (matching of coeval events of mafic magmatism between blocks) and determination of the apparent polar wander paths, these studies provide a better understanding of the position of continents and supercontinents in the past. The robust U–Pb baddeleyite age of 1922 ± 6 Ma for the RP353 dyke of the Tsineng Swarm in the western Kaapvaal Craton, obtained in this study, establishes a link between the Tsineng Dyke Swarm and the 1928 ± 4 Ma Hartley Basalt Formation, as well as ca. 1927 Ma dolerite sills intruding the Waterberg Group (Moshaneng dolerites). The comparison of barcode diagrams for the Kaapvaal and Zimbabwe cratons can constrain the timing of the collision between the two cratons to ca. 1.92 to ca. 1.88 Ga, though future studies are required to confirm this inference. Paleomagnetic data for 77 drill core samples from the Hartley Basalt Formation of the Olifantshoek Supergroup in western Kaapvaal Craton, provides a paleomagnetic pole (N°= 22.7, E°=328.6, α95=11.7) for the primary remanence direction. The new robust paleopole for the Hartley Basalt Formation fits well with in the existing Paleoproterozoic polar wander path of the Kaapvaal craton. Geochronology, paleomagnetism and geochemistry of the 1.93 – 1.92 Ga and 1.88 – 1.84 Ga rocks in the Kaapvaal Craton points towards two separate magmatic events.

Keywords: Kaapvaal, Tsineng, Hartley, baddeleyite, U-Pb geochronology, paleomagnetism, polar wander path, Kalahari

Supervisor(s): Ulf Söderlund (Lund University) and Michiel de Kock (University of Johannesburg)

Subject: Bedrock Geology

Farnaz Alebouyeh Semami, Department of Geology, Lund University, Sölvegatan 12, SE-223 62 Lund, Sweden. E-mail: f.alebouyeh@gmail.com

U-Pb åldersdatering av Tsineng diabasgångsvärmen och paleomagnetiska studier av Hartley Basalt Formationen, Sydafrika – bevis för två separata magmatiska händelser för 1.93 – 1.92 och 1.88 – 1.84 miljarder år sedan i Kalahari

FARNAZ ALEBOUYEH SEMAMI

Alebouyeh Semami, F., 2014: U-Pb åldersdatering av Tsineng diabasgångsvärmen och paleomagnetiska studier av Hartley Basalt Formationen, Sydafrika – bevis för två separata magmatiska händelser för 1.93 – 1.92 och 1.88 – 1.84 miljarder år sedan i Kalahari. *Examensarbeten i geologi vid Lunds universitet*, Nr. 416, 30 sid. 45 hp.

Abstrakt: Geokronologi och paleomagnetiska studier är de viktigaste verktygen för paleogeografiska rekonstruktioner kring hur kontinenter fårhållit sig relativt till varandra under geologisk tid. Genom att jämföra s.k. polvandringskurvor och tidpunkter för storskaliga magmatiska händelser mellan olika krustala block (kontienter/ kratoner) kan vi få en bättre förståelse av hur dessa block förhöll sig relativt till varandra under tidsperioder då superkontinenter existerade. I denna studie åldersbestämdes en diabasgång från Tsineng diabasgångsvärmen till 1922 ± 6 Ma (U-Pb metoden på mineralet baddeleyit). Denna gångsvärm återfinns i västra Kaapvaal, och denna ålder indikerar ett samband mellan Tsinenggångsvärmen och den tidigare daterade (1928 ± 4 Ma) Hartley Basalt Formationen samt talrika diabasgångar i Waterberg Group (ca 1927 Ma, ”the Moshanengdiabases”). Jämförelse av tidpunkter för basisk magmatism i Kaapvaal och Zimbabwe kratonerna indikerar att tidpunkten för kollisionen mellan de två kratonerna sannolikt skedde mellan ca 1.92 och ca 1.88 Ga. Paleomagnetisk data från 77 borrkärnsprover från Hartley Basalt Formationen i västra Kaapvaal kratonen, ger en paleomagnetisk pol (N°= 22.7, E°=328.6, α95=11.7) för den primära remanens riktningen. Denna nya och mera exakta paleopol för Hartley Basalt Formationen faller väl inom den befintliga polvandringskurvan för Kaapvaal för denna tidsepok. Geokronologi, paleomagnetism och geokemi av 1.93 – 1.92 Ga och 1.88 – 1.84 Ga bergarter i Kaapvaal kratonen pekar mot två separata magmatiska händelser för dessa generationer.

Nyckelord: Kaapvaal, Tsineng, Hartley, baddeleyite, U-Pb geokronologi , paleomagnetism, polar wander path, Kalahari

Handledare: Ulf Söderlund (Lund University) and Michiel de Kock (University of Johannesburg)

Ämne: Berggrundsgeologi

Farnaz Alebouyeh Semami, Geologiska institutionen, Lunds Universitet, Sölvegatan 12, 223 62 Lund, Sverige.
E-post: f.alebouyeh@gmail.com

1 Introduction

Precise and well-constrained paleopoles are key factors in paleogeographical reconstruction and together with geochronological data they can provide us with the history of plate tectonics and the position of continents and supercontinents in the past. This knowledge will lead to recognition of the provenance sources, help in tracing sedimentary basins and metallogenic belts in between cratonic blocks. Our findings about Archean crust and magmatic sills, dykes and layered intrusions of Large Igneous Provinces (LIPs) are disseminated. LIP is a term which refers to the continental flood basalts and their oceanic equivalent, massive oceanic plateaus.

Achieving a precise age for these intrusions leads to the creation of barcode diagrams (Fig. 1), an efficient tool to correlate and match different fragments of the crust and obtain a picture from the time before and after the cratons had detached from each other. In a barcode diagram, each bar represents a regional magmatic event.

The RP353 dyke is one of NE-trending dykes of the Tsineng dyke swarm, and it is located at the western domain of Kaapvaal Craton. In this study a geochronological dating performed on this dyke has yielded the age 1.92 Ga, indicating that the Tsineng dyke swarm belongs to an extensive mafic magmatic event that includes coeval units of Hartley Baslat Formation and the older pulse of the post-Waterberg sills. With the sampling of fresh outcrops of the Hartley Basalt Formation, it has become possible to obtain an undisturbed paleo-magnetic pole that has used to constrain a robust paleopole for the Kaapvaal Craton at the time of the emplacement of the RP353 dyke.

For years, the relation between Kaapvaal and Zimbabwe cratons and the exact timing of the formation of the Kalahari craton has been the subject of many debates. According to some earlier studies such as Söderlund et al. (2010) which has precisely matched the dyke swarms and regions in both cratons or Barton et al., (1994); Holzer et al., (1998) that has studies the central zone of the Limpopo belt based on dating of metamorphic zircons, we can say that the majority of the workers agree that the Kalahari craton was formed sometime after 2.0 Ga. However, in conflict with previous studies, Hanson et.al (2011) has suggested that based on a U-Pb geochronology of mafic units and paleomagnetic data of the South Africa and Zimbabwe rocks, at 1.88 Ga the cratons must have been at least 2000 km apart.

Main objectives of this study are:

1. Obtaining a precise age and paleomagnetic data for RP353 (and other possible coeval units) to test relative positions of Kaapvaal and Zimbabwe cratons at ca. 1.92 and 1.88 Ga.
2. Investigating the extent and possible tectonic setting of ca.1.92 Ga mafic magmatism in northern Kaapvaal Craton and discuss a possible relation to the slightly younger pulse of magmatism (ca. 1.88 Ga).
3. Testing the relative positions of Kaapvaal and Zimbabwe Cratons at ca.1.92 and 1.88 Ga and analyzing Hanson el al.,'s theory about 2000 km distance between cratons.

2 Geological setting

2.1 Regional geology

Located partialy in northern South Africa, Swaziland and Botswana, Kaapvaal Craton is one of the oldest (3.7 – 2.5 Ga) and most well-preserved cratons in the world (Fig. 2). Together with Zimbabwe Craton they comprise the much larger Kalahari Craton, which is

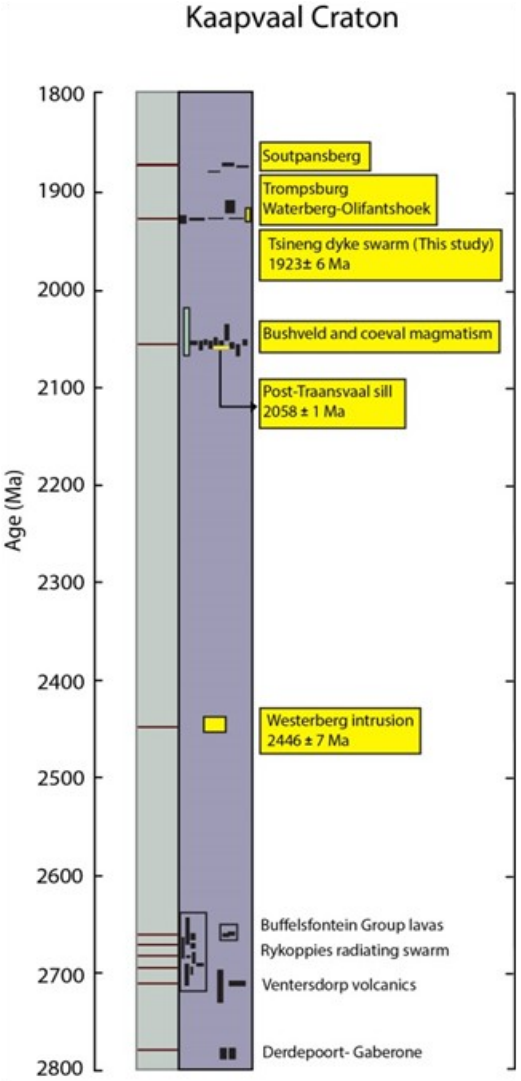

Fig. 1. LIP barcode diagram for the Kaapvaal Craton. The geochronological ages are extracted from Hanson et al. (2004), Ernst and Buchan (2001) and Olsson et al. (2010, 2011).

believed to be the result of a collision along the Limpopo belt presumably at ca. 2.0 Ga (Jacobs et al. 2008; Söderlund et al., 2010; Hanson et al., 2011). Kaapvaal Craton is truncated by the Limpopo Belt in north, Namaqua–Natal Proterozoic mobile-belt (ca. 1.1 – 1.9 Ga) in south, the Kheis over-thrust belt (ca. 2.0 Ga, James et al., 2003) in west and Lebombo monocline in east. Shield of the Kaapvaal Craton is composed of greenstones and granitic terranes. Cratonic basins has deveoped on top of this shield and the presence of mobile belts reflects the re-working of the shield and in some cases the cratonic basins in linear zones (Hunter, 1974).

The Kaapvaal Craton is dominated by Meso-Archean basins, with sedimentary successions intruded by Neo Archean granites. Primary stages of crust formation are from 3.7 Ga to around 3.1 Ga, followed by a period of crustal stabilization from 3.1 to 2.6 Ga. However, evidence of less extensive activities during this period can be found in several areas. The Kaapvaal Craton can be divided into two main domains. A western domain with supercrustals mainly younger than 3.1 Ga (3.1 – 2.6 Ga) that unconformebly overlay 3.6 – 2.9 Ga granites and greenstones of the older eastern domain (James et al., 2003; Bumpy et al., 2011). The Greenstone belts (3.7 – 3.1 Ga) assiociated and gneisses (with 3.68 – 3.2 Ga protolith ages) together within the Swaziland Block are located in the south-eastern domain of Kaapvaal Craton. Along the northern fringe of the southeastern domain, the Barbertone Greenstone Belt (3.57 – 3.08 Ga) is placed which is believed to be the core that later formed Kaapvaal Craton (Eglington and Armstrong, 2004). At 3.07 Ga extensive uplift and weatheing of granites and greenstones led to the deposition of volcanics and clastic sediments of the Dominion Group (Fig. 1). Deposition of Pongola sediments and volcanics occured at 3.0 – 2.9 Ga in southeastern part of the Kaapvaal Craton, followed by the formation of Witwatersrand (overlying Dominion Group lithologies) and Ventersdorp Supergroups along the eastern margin of this craton between 2.9 – 2.7 Ga (Griffin et al, 2003). Transvaal Supergroup unconformably lies on top of the volcano-sediments of Ventersdorp Group. Ventersdorp (ca. 2.7 Ga) and Karoo Groups (ca. 0.2 Ga) together with the sands of Kalahari desert, cover a large area of 3.0 – 2.8 Ga granitic gneisses and unfoliated granitoids (ca. 2.65 with interbeddings of 3.0 – 3.1 Ga thin greenstone belts) in the western domain of the craton. The amalgamation and of Kaapvaal's two domains happened around 2.5 Ga (Griffin et al., 2003, Schmitz et al., 2004).

Pietersburg terrane (2.9 – 2.6 Ga) is located in the center of Kaapvaal Craton and consists of massive granites and granodiorites together with tonalitic (in some cases trondhjemitic) gneisses. The Bushveld complex took place at ~2.06 Ga at the northern part of the central domain (Olsson et al., 2011). Some studies state that at around 2025 until 1990 Ma a collision between Kaapvaal and Zimbabwe Cratons resulted in the formation of Magondi-Limpopo belt and a metamorphic overprint on the granulites of Limpopo area, however this theory has been challenged by Hanson, proposing a 2000 km distance between two Cratons at 1.88 Ga (Hanson et al., 2011).

In addition, 1990 Ma age yielded from the detrital zircons from Sandriviersberg formation (Waterberg Group) may point towards the fact that upper Waterberg Group can be the foundation of the rocks of Magondi-Limpopo belt. A rifting event along the western edge of Kaapvaal Craton between 1930 and 1850 Ma, led to the deposition of lower formations of Soutpansberg and Palaye Group. Along the Limpopo Belt and at the northern margin of Kaapvaal Craton, upper formations of Soutpansberg Group were deposited during 1850 – 1800 Ma. By this time the western margin of Kaapvaal Craton had turned into a passive margin and the formation of Grobleshoop Group of Kheis Supergroup was taking place (Dorland, 2009).

2.2 Local geology

2.2.1 Olifantshoek Supergroup

From Boegoeberg Dam on the Orange River (Northern Cape Province of South Africa) towards the north and reaching Korannaberg Mountains, The Olifantshoek Supergroup is noticeable in form of a distinct mountain range (Fig 3). Aeromagnetic data and location of out crops together with various drill-cores from this area has indicated a north trending strata stretching towards Zoetfontein fault (Moen, 2006). The most well-defined boundary between the Kheis Province and the Kaapvaal Craton is at the base of Olifantshoek Supergroup and its type locality is situated within 20 km west of the town Postmasburg (Cornell et al. 1998).

Deposited as clastic and fluvial deposits along the western margin of the Kaapvaal Craton, the Olifantshoek Supergroup is made up of basic lava, quartzite and interbeds of shale which are overlain by a thick succession of coarse-grained quartzite (with red and grey color) and some shale (Fig. 3, Table 1). The sediments of Olifantshoek Supergroup overlie unconformably sediments of Transvaal Supergroup. The entire sediments of the Olifantshoek Supergroup have undergone very low to low grade metamorphism, folding and low-angled thrusting (eastwards) related to Kheis orogenic activity. The intensity of the folding increases towards the west and causes the folds to have steep limbs and dip eastwards (Moen, 2006).

The Olifantshoek Supergroup begins with Mapedi and its equivalent Gamagara Formation at the bottom, over the unconformity that covers the Postmasburg Group of the Transvaal Supergroup and ends with its last formation, Vuilnek formation at the top. Manganese and iron ore deposits can be found along the western limb of the Maremane anticline, just below

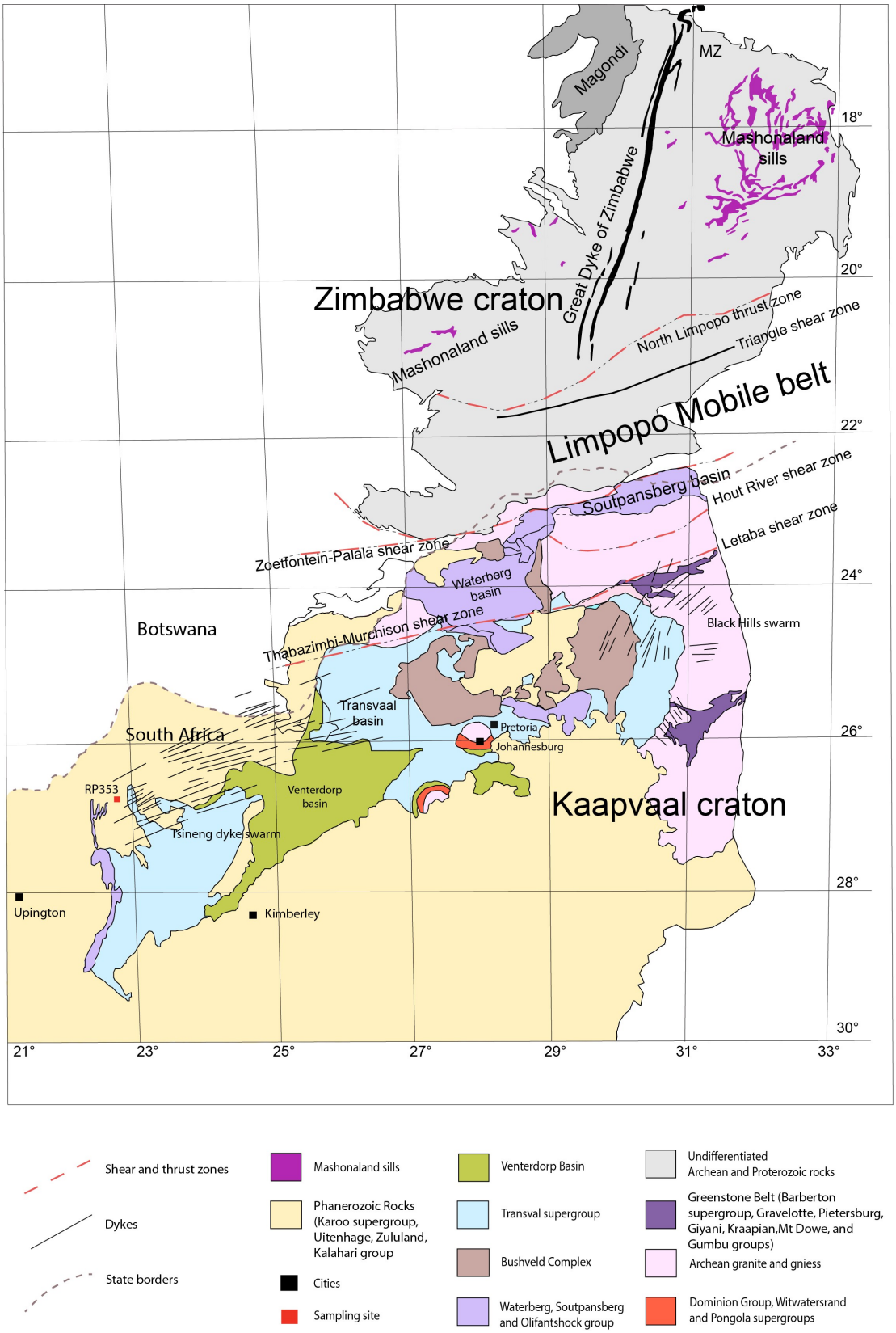

Fig. 2. Regional map of Kaapvaal and Zimbabwe cratons showing the major Archaean to Proterozoic lithological units. Also shown are the Tsineng dyke swarm and geochronological sampling site, RP353 dyke. For Zimbabwe Craton units units of the 1880 Ma Mashonaland LIP and the 2575 Ma Great Dyke of Zimbabwe LIP are shown.

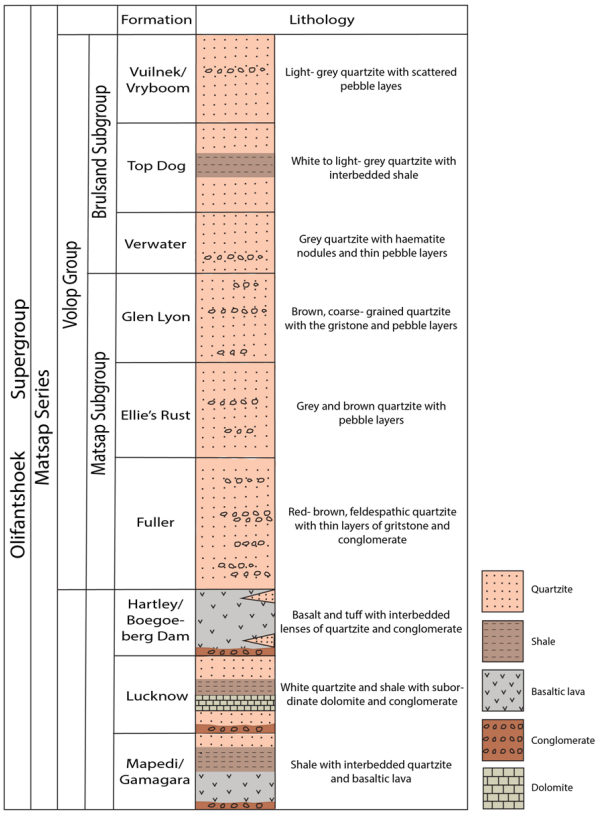

Fig. 3. Subdivision and schematic lithology of the Olifantshoek Supergroup.

Table 1. Stratigraphic subdivision and Lithology of the Olifantshoek Supergroup (Modified from Cornell, 1987)

Lithology of the Olifantshoek Supergroup

	SACS (1980)		Main Lithology	Rogers (1906)	
KheisSupergroup	Groblershoop		Quartz-mica schist		
OlifantshoekSuper group	Volop Group	Brulsand	Light grey quartzite	Upper Beds	Matsap Series
		Matsap	Brownish quartz arenite		
	Hartley		Basaltic lava and tuff (andesite of SACS)	Middle or Hartley Hill Beds	
	Lucknow Formation		Brown and white quartz arenite (SACS: no brown)	Lower Beds	
	Mapedi/Gamagara Formation		Shale, slate, breccia		

the Gamagara formation. These ore deposits are the consequence of an erosion period prior to the formation of the Olifantshoek Supergroup.

The Mapedi formation was deposited in a deep shelf environment associated with mafic volcanism and comprises quartz-rich sediments, mafic volcanics and shale. The Lucknow formation is on top of the Mapedi formation and was deposited in a shallow-marine environment with repeated stages of transgression and regression. It is characterized by quartzite and $\delta^{13}C$ carbonates (van Niekerk, 2006). The Neylan conglomerate layer at the bottom of Hartley Formation overlay an unconformity which separates the shallow-marine sediments and carbonates of the Lucknow Formation from the upper sequences. This unconformity is believed to have formed during an earlier distortion of the crust before the rifting event (the event that it is believed to have formed Hartely Lava) along the recently evolved western margin of Kaapvaal Craton. Hartley lava transitions gradually to the overlaying quartzites of Volop Group (Olifantshoek Soupergroup), deposited in a braided river environment. Volop Group devides into two main series, Matsap and Brulsand each including three members. In the Matsapseries, the feldespatic quartizes of Fuller member gradually transitions to a finer grained member named Elli's Rust which then grades upwards into Glen Lyon member with coarser grains. The Bruslandseries starts with the basal Verwater member which grades into the Top Dog member dominated by mature quartizes and orthoquartizes (quartzite with a sedimentary origin and lacking fine-grained matrix). Sediments of the Top Dog member are the indication of a change in the depositional environment from fluvial (characteristic of Volop Group) to shallow-marine Groblershoop Group of Kheis Supergroup (overlying Olifantshoek Group) (van Niekerk, 2006).

2.2.1.1 Matsap Series

Deposition of immature quartz arenites and wackes, found in Matsap Formation, Waterberg and Soutbansberg Groups is related to a subsidence event following deep crustal faulting. Initial correlation between the red beds of Matsap (quartz arenites) and equivalent units in Transvaal basin, Zimbabwe and Botswana were made by Du toit, 1926 (Cornell, 1987).

2.2.1.1.1 Hartley Basalt Formation

Hartley Basalt formation is located in the western margin of Kaapvaal Craton, northern Cape Province in South Africa. This formation was first introduced by Rogers in the year 1906, describing this layer as "Middle beds or Hartley Hill group" of Mastsap series. He identified the type section of the Hartley formation and also put out a stratigraphic section of this formation. Later, Du toit (1926) presented the regional correlation of redbeds of quartz arenite belong to Matsap series with the similar units in Zimbabwe, Botswana and Transvaal basin. In 1998, Cornell studied the area, sampled and dated Hartley Basalt formation (1928 ± 4 Ma, Cornell, 1998) and stated that the formation consists of basalt, tuff and tuffaceous quartz arenite, wacke conglomerate with a volcanic matrix and quartz-feldspar porphyry (out crop in Pramberg). It is believed that the deposition of Hartley formation has occurred during a period of bimodal volcanic activity resulted by a continental rifting system, along the western fringe of Kaapvaal Craton (van Niekrek, 2006). The deposition of the Hartley formation signifies the initial phase of continental rifting prior to the stabilization of the western margin of the Kaapvaal Craton (Fig. 4).

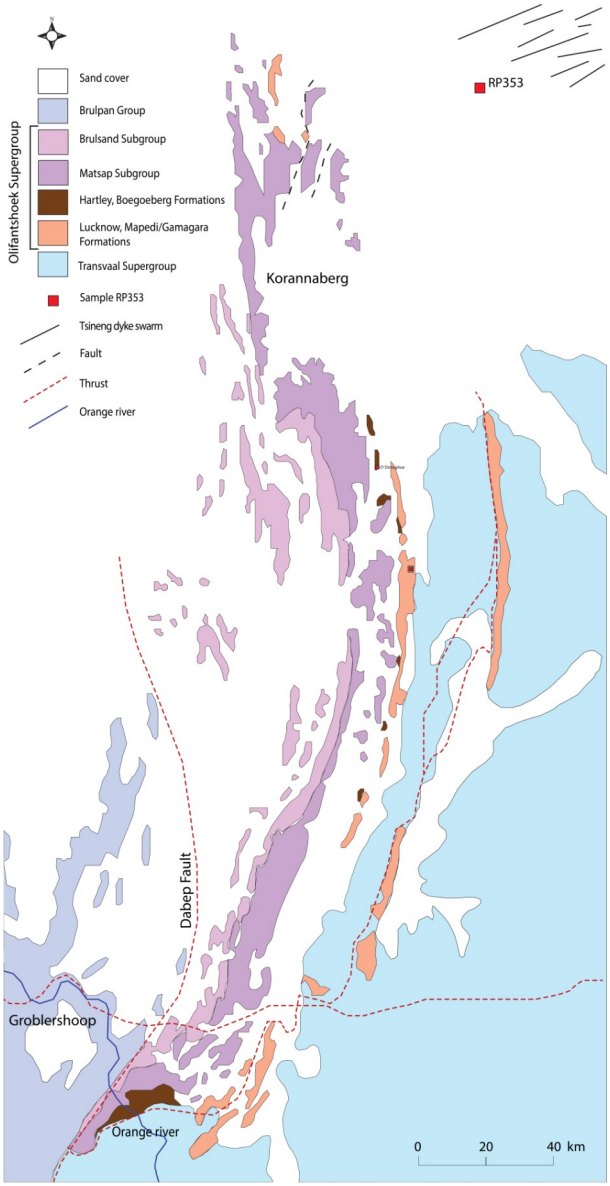

Fig. 4. Detailed map illustrating the location of the Olifansthoek Supergroup and it's main subdivision, as well as showing the RP353 sampling site for geochronology.

2.2.2 Tsineng Dyke swarm

This mafic dyke swarm is located in the Northern Cape Province of South Africa penetrating the western side of Kaapvaal Craton (Fig. 2). The Tsineng swarm is distinct on aeromagnetic maps and displays a slight convergence towards the WSW, pointing towards a potential magmatic center (plume) (Goldberg, 2010). At the western end of the craton the swarm is truncated by the Kheis fold belt therefore predating the Kheis orogeny (ca. 1.8 Ga). Tsineng swarm fans out toward ENE and the strike of its axis is ~070° in the east with a slight dextral curvature and ~060° in the west. Aeromagnetic data indicates that these dykes crosscut the 2222 Ma Ongeluk Lava of the Postmasburg Group presenting the maximum age constrain, and a minimum age constrain is presented by 1928 Ma Hartley Lava (Cornell et al., 1998) of the Olifantshoek Supergroup (Goldberg 2010).
Goldberg (2010) interprets this swarm as a failed arm of a rift systemprior to the intrusion of the dykes, in the western Kaapvaal Craton that is linked to the 1928 Ma Hartley. This is similar to the earlier idea of Cornell (1987) who suggested that the Waterberg and Soutpansberg groups occupy a failed arm setting with a triple junction located on the west side of the Kaapvaal Craton.

2.2.2.1 The RP353 sample

The drill core sample RP353 was extracted from one of the NE trending dykes within Smartt Mine, Tsineng dyke swarm, located in the Kalahari manganese field (Fig. 4). The host rocks are the manganese-rich rocks from Hotazel Formation (Upper Transvaal Supergroup) and lie conformably between the Ongeluk volcanic rocks and the dolomitic Moodraai Formation of the same Supergroup (Evans et al., 2001). The Hotazel Formation has experienced slight folding, low grade hydrothermal and supergene alteration, and also metamorphism (Beukes and Gutzmer, 1996). These events took place shortly after ~2.22 Ga, and resulted in a primary occurrence of manganese ore genesis. The supergene alteration event did not disturb the dykes of this region; however, it might be the reason in local progression of manganese ore. The RP353 sample is a coarse grained dolerite with plagioclase phenocrysts.

3 Geochronology: Methodology and analytical techniques

3.1 TIMS Baddeleyite U-Pb geochronology

The drill core RP353 intersected the Tsineng Dyke Swarm (near the town Tsineng, in the Northern Cape Province of South Africa) was sampled by Michiel De Kock from the University of Johannesburg. Baddeleyite grains (~30 µm) were extracted after crushing, milling and separation using the Wilfley Table at Lund University following the procedures described in Söderlund and Johansson (2002). The dolerite sample was crushed into 1 cm^3 size pieces using a sledge hammer, and then placed into a ring, chrome-steel mill to obtaina fine powder (~3 – 4 µm). For each loading of the powder, caution was taken to suspend it in a small amount of water prior to placement on the Wilfley Table. Due to the small size of the baddeleyite grains, the material was collected from the table a fraction earlier than normally stipulated in Söderlund and Johansson (2002). Baddeleyite grains tend to gather as the final visible mineral trace on the Wifley Table according to Söderlund and Johansson (2002). The final visible mineral trace was washed off the Wifley Table using a water bottle and collected in a 5L plastic

beaker. After 2 – 3 loadings, the grains were transferred into a small petri dish after having been cleaned in hot water and Ethanol. Before separating the baddeleyite grains from the collected sample, magnetic minerals were extracted using a pencil shaped hand-magnet wrapped in plastic. The best-quality baddeleyite grains were then hand-picked under a binocular microscope, using a pair of tweezers and a handmade micro-pipette. The grains were then transferred into another clean petri dish without any other minerals, such as apatite. The grains are ~30 µm and clear (not alerted) with light brown color.

In clean laboratory ethanol was added to each petri dish and baddeleyite grains were divided into three fractions composedof 9, 12 and 16 grains each. The grains were transferred into Teflon dissolution capsules using a hand-made micro pipette. All grains were repeatedly washed in MQ-H2O in order to dilute the amount of Pb blank (procedural Pb blank was 1 to 5 pg). On a hot plate,the grains were repeatedly washed for ~20 minutes followed by several washing steps in 3N HNO3 and subsequently MQ-H2O. After all the solution was removed, one drop (~5 ml) of a tracer solution ($^{233-236}$U-^{205}Pb), 10 drops of HF and one drop of HNO3was added to each Teflon capsule. All grains were dissolved over a period of 3 days in the oven under high pressure and 210°C temperature.

After this dissolution, all of the solution was evaporated on a hot plate at a temperature of 100°C for approximately 2 hours. In order to convert the fluorides to chlorides, all samples were then re-dissolved in 10 drops of 6.2N HCl followed by one drop of H3PO4 and left on the hot plate to dry down (~85°C) for about an hour. Zr-Hf-REE fractions were washed out by using HF and HCl in earlier steps. Afterwards sample-drops were loaded to 50 µl columns filled with previously cleaned anion exchange resin (with Bio Radof 200 – 400 mesh chloride). U and Pb were washed out with H2O and collected into the dissolution Teflon capsules. 2 µl of silica gel, produced according to Gerstenberger and Haase (1997) formula, was used for dissolving the concentrated H3PO4 and sample-drop prior to loading on an outgassed Rhenium (Re) filament. The sample-drops with silica gel were dried down using a filament current of 1 A, followed by a slow increase (to ~2.3 A) where all the H3PO4 was vaporized. The loading procedure ended with a slow final filament current rise until a weak orange glow on the Re filament could be seen.

Thermal Ionization Mass Spectrometry (TIMS) analysis was performed using a Finnigan Thermal Mass Spectrometer, equipped with a Secondary Electron Multiplier (SEM) in the Laboratory of Isotope Geology at the Swedish Museum of National History in Stockholm. Data was plotted using the Excel Add-in software Isoplot (Ludwig, 2003). Uranium decay constants used, were those published in Jaffey et al. (1971). The correction for initial common lead was carried out using the isotopic model compositions of global common lead taken after Stacey and Kramers (1975).

3.2 Results

Baddeleyite grains, extracted from the RP353 core sample do not show any sign of rust or alteration and appear to be clear with light brown color. The three fractions plotted on the Concordia diagram, yields a robust age of 1922 ± 6 Ma (Fig. 5) for the RP353 dyke of the NE-trending Tsineng dyke swarm. This result indicates that both ^{206}Pb/^{238}U and ^{207}Pb/^{235}U ratios show a similar concordant age and the fractions plot perfectly on the Concordia line. The accuracy of this measurement is indicated by the MSWD value of 0.04. The U-Pb TIMS data is presented in Table 2.

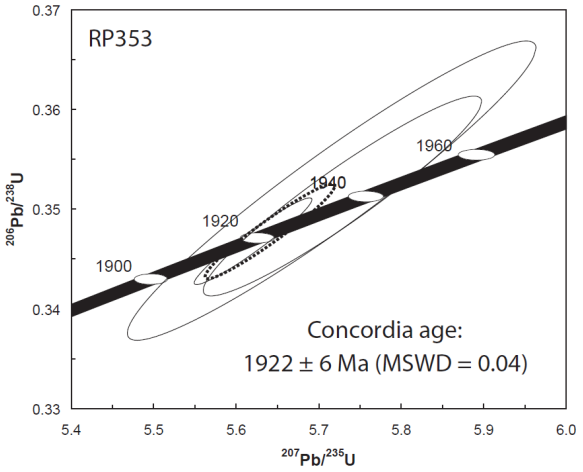

Fig. 5. U-Pb Concodria diagram for the sample RP353. The three fractions are marked with grey ellipses, whereas the concordia age is defined by ellipse with dashed border. Data point error ellipses are 2σ.

4 Paleomagnetism: Methodology and analythical techniques

4.1 Paleomagnetism: sampling and labratory processing

A series of sites (HAA-HCA) were drilled and sampled by Farnaz Alebouyeh (Lund University), Michiel de Kock and Ashley Gumsley (University of Johannesburg) for paleomagnetic studies. From each unit at every site 8 to 9 samples were drilled using a water- cooled portable drill (Fig. 6). Samples HAA to HAH were extracted from the Hartley Hill quarry (Fig. 7a, b), outside of the town of Olifantshoek. The Hartley Hill quarry was chosen as the main sampling site since it includes a continuous occurrence of undeformed and minimum altered Hartley Basalt (over 500 m^2) and a great exposure of eight sub-horizontal lava flows (Evans et al., 2002).

Table 2. U-Pb TIMS data.

Analysis no. (number of grains)	U/ Th	Pbc/ Pbtot[1)]	$^{206}Pb/^{204}Pb$ raw[2)]	$^{207}Pb/^{235}U$	± 2s % err	$^{206}Pb/^{238}U$ [corr][3)]	± 2s % err	$^{207}Pb/^{235}U$ [age, Ma]	$^{206}Pb/^{238}U$ [age, Ma]	$^{207}Pb/^{206}Pb$ [age, Ma]	± 2s	Concord-ance
Bd-1 (9 grains)	4.7	0.428	121.5	5.7148	3.54	0.35170	3.51	1933.6	1942.7	1923.9	19.6	1.010
Bd-2 (12 grains)	5.8	0.213	286.3	5.7282	2.41	0.35119	2.35	1935.6	1940.3	1930.7	14.3	1.005
Bd-3 (16 grains)	4.6	0.075	828.4	5.6202	1.04	0.34661	1.03	1919.2	1918.4	1920.1	5.2	0.999

[1)] Pbc = common Pb; Pbtot = total Pb (radiogenic + blank + initial).

[2)] measured ratio, corrected for fractionation and spike.

[3)] isotopic ratios corrected for fractionation (0.1% per amu for Pb), spike contribution, blank (1 pg Pb and 0.1 pg U), and initial common Pb. Initial common Pb corrected with isotopic compositions from the model of Stacey and Kramers (1975) at the age of the sample.

Fig. 6. All samples were drilled using a water-cooled portable drill.

Samples from HBA were drilled from a site at the Pramberg quartz porphyry (Fig. 8a) located outcropping at a small hill to the south east of north-south trending quartzite ridges. Lastly, HCA samples were obtained from a site located on the O'Donoghue Farm (Fig. 8b). Further information on the sampling sites is presented in Table 3.

Sample preparation, including the cutting of 1 cm^3 cylindrical cores and labeling was completed at the University of Johannesburg's paleomagnetic laboratory.

In total, 77 core samples between three and ten cm long were drilled from each site using a portable petrol-powered water-cooled diamond drill. For all the units sampled at each site, geographic orientation, including azimuth and inclination was measured using an orientation sleeve equipped with both a sun and a magnetic compass with inclinometer and the exact time of taking the measurements was carefully recorded (Fig. 9a). The samples were marked with a brass or copper wire through a slot. An arrow showing the direction of drilling was drawn on the side of the sample and samples were named with a permanent black marker according to procedures by Tauxe (2007) (Fig. 9b). When finished with measurements, cores were removed using a hammer and a chisel. Orientation values (strike and dip) were recorded for each lava flow.

In paleomagnetism laboratory at the University of Johannesburg, all samples were cut into two to three

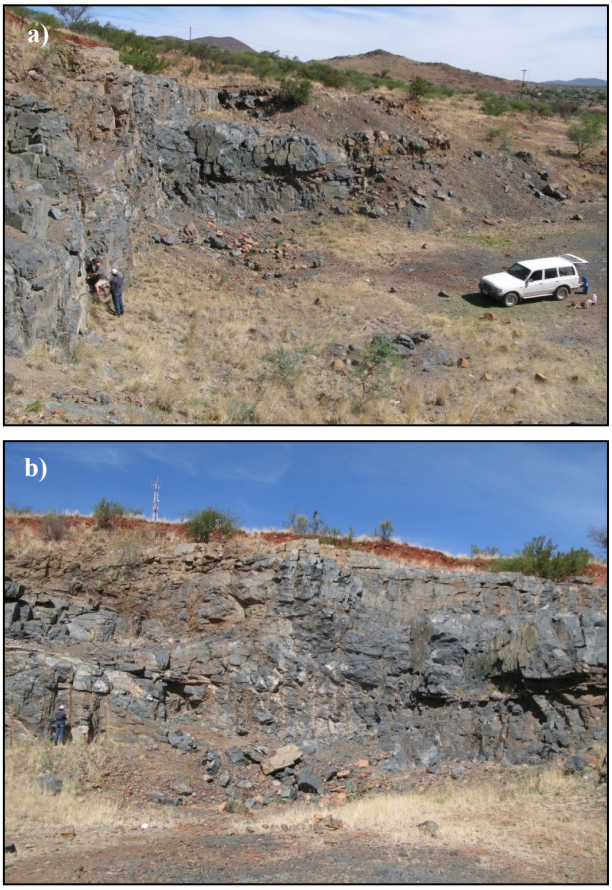

Fig. 7. a) The Hartley Hill quarry, the main sampling locality for paleomagnetic analysis (to the left). b) The profile of the Hartley Hill quarry (to the right). Samples HAA-HAH were extracted from this locality.

specimens of 1 – 2 cm and duplicates were saved aside for the future Thermal demagnetization process (Fig. 10b), if desired. Broken samples were glued and labeled with a white correction pen (Fig. 10a). Due to the slight discrepancy between sun compass and magnetic compass readings, the data was corrected prior to the demagnetization procedure. The process of demagnetization and magnetic remanence measurements were carried out by a superconducting rock magnetometer (vertical 2G Enterprises DC-4K with three axes SQUID sensors) at the University of Johannesburg.

Table 3. Localities and lithology of samples.

Site	Coordinates (°S,°E)	N	Bedding(strike/dip)	Lithology
HAA	27°056.067"S 22°045.311"E	9	111°/22°	Basalt
HAB	27°056.067"S 22°045.311"E	8	111°/22°	Basalt
HAC	27°056.067"S 22°045.311"E	7	111°/22°	Amygdaloidal Basalt
HAD	27°056.067"S 22°045.311"E	4	111°/22°	Grayish Tuff
HAE	27°056.067"S 22°045.311"E	8	111°/22°	Basalt
HAF	27°056.067"S 22°045.311"E	8	111°/22°	Foliated , dark Basalt- Epidote in foliation planes
HAG	27°056.067"S 22°045.311"E	8	111°/22°	Pyroclastic/Tuffaceous with interbedded lava flows
HAH	27°056.067"S 22°045.311"E	8	111°/22°	Basaltic Lava with higher Epidote content
HBA	27°052.199"S 22°045.010"E	9	130°/53°	Reddish Quartz and Feldspar Porphyry
HCA	27°052.199"S 22°045.010"E	8	120°/62°	Foliated, greenish and high schistose lava

Fig. 8. a) Quartz porphyry deposits in Pramberg area. HBA samples were extracted from this locality. b) Foliated and high schistose greenish lava from O'Donoghue farm, where HCA samples were extracted from.

Fig. 9. a) The orientation sleeve equipped with a sun compass, a magnetic compass and inclinometer. b) Core samples were marked in order to specify the direction of drilling.

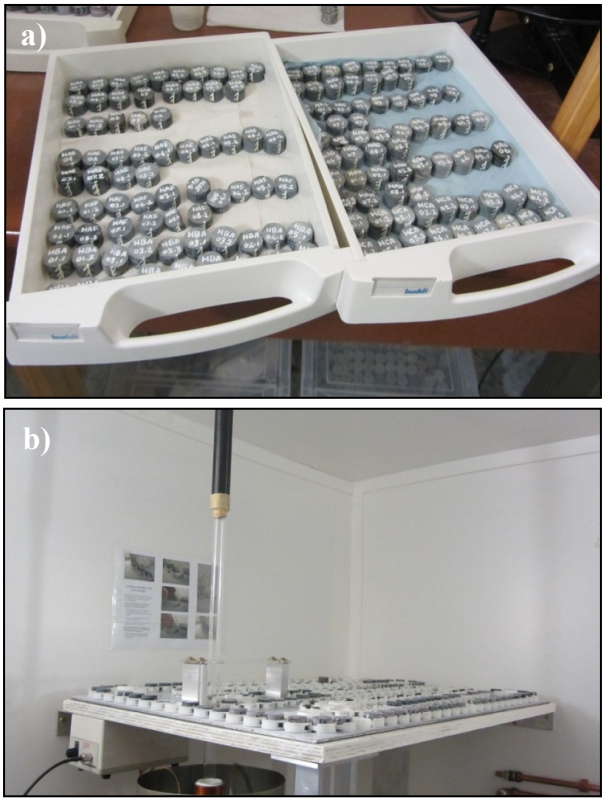

Fig. 10. a) Marked specimens ready to be loaded into the magnetometer. b) Specimens loaded into the magnetometer's trey and ready for AF demagnetization procedure.

Each rock sample that is extracted from a geological formation has a Natural Remnant Magnetism (NRM in short) that can generate as a result of natural phenomena (lightening etc.) or manmade procedures like sampling and different stages of preparation process (Tauxe, 2007). Therefore, the demagnetization process began with the measurement NRM followed by a stepwise demagnetization process consisting of low and high alternating field (AF) demagnetization. AF demagnetization was performed with the help of a high-field degausser that is in accordance with the magnetometer.

The steps of the low AF demagnetization process were defined as 2.5, 5.0, 7.5 and 10.0 mT followed by five additional steps 15.0, 20.0, 25.0, 30.0, 35.0 and 40.0 mT. High AF demagnetization consisted of eight steps including 45.0, 50.0, 55.0, 60.0, 65.0, 70.0, 75.0, 80.0 mT. In the end, the last resistant and consistent samples were exposed to extra high AF steps, 85.0, 90.0, 95.0, 100.0 mT, in order to be fully demagnetized. The samples that showed a strong resistance to demagnetization (in this case HAH) were drowned in a sufficient amount of liquid nitrogen in order to mitigate their resistance (Fig. 11 a, b). After this process the measurements steps were performed in the same manner for these specimens. The process was terminated after the specimens started to behave unstably and their magnetic intensity dropped lower than the one of sample holder tube of the magnetometer.

4.2 Results

4.2.1 Demagnetization behavior and components

Intensity and orientation measurments of the remanent magnatism during a graduational demagnetization process (Alternating field or AF from 2.5 to 100 milli-Tesla in this study) constitues magnetic vectors. The tip of a magnatic vector remaining after each demagnetization step represents a point in the three- dimensional magnetic projection. The magnetic history (i.e., through the identification of recorded magnetic components) of each specimen can be obtained by the interpretation of all these points (Kirschvink, 1980). Identification and inerpretation of the magnatic components were completed by Kirschvink's least-squares principal-component analysis (Kirschvink, 1980), using the Macintosh™ based computer program Paleomag 3.1b2 (Jones, 2002). Reconstruction of the paleomagnetic pole in the next section was accomplished using G-plates 1.2.0 the interactive plate-tectonic reconstructions and visualisations software (2003).

The sampling sites at Hartley Hill largely overlap with the sites of Evans et al (2002). During their study Evans and co-workers only collected four samples per site (or lava flow unit). In this study 8 additional samples was collected from each unit, with the exception of site HLO4 of Evans et al. (2002) that was not

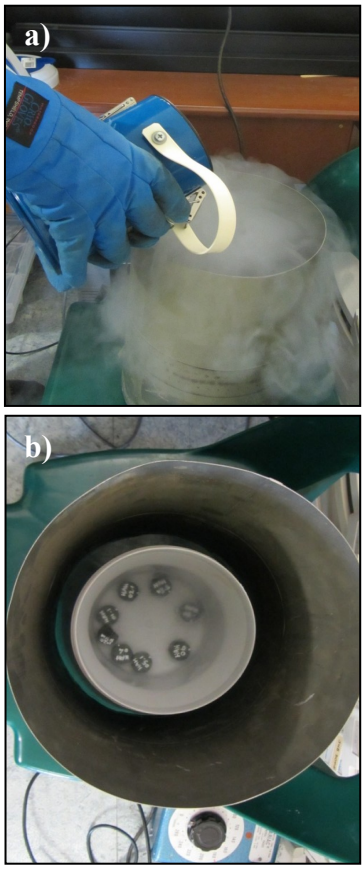

Fig. 11. a, b) The HAH specimens were drowned in liquid nitrogen to reduce their magnetic resistance.

sampled. Interbedded pyroclastic material sampled suring the current study provides an additional site (i.e., HAD). In total nine units were sampled at Hartley Hill during this study and that of Evans et al. (2002). The demagnetization results of Evans et al (2002) is combined with those of this study for the calculation of combined site means.

Vector endpoints in most samples exhibit well-defined linear trends, and at high demagnetization fields these vector end points define either linear trends towards the origin or clump together as stable endpoints of demagnetization. Linear fits were obtained for all components. For those that trend towards the origin, the origin was included in the fit. Linear fits through stable endpoints were included the origin and were forced through the origin. In all cases linear fits were accepted if their maximum angular deviation (MAD angle) was less or equal to 10°. In a few cases demagnetization at high fields defined linear trends that both missed the origin and failed to form stable endpoints. In these cases a higher stability component of magnetization failed to demagnetize. Great cirlcle paths were fitted in these cases to quantify the remaining components. The same software was used in order to determine Fisher statistics for the least square analysis (Table 4). With the comparison of the statistics for each component from the various sampling sites, it is possible to achieve the mean paleomagnetic direction and corresponding paleopole position. The details of least squares analyses and Fisher statistics for all the sampling sites and a summary of low and high coercivity components are provided in Table 4. It is siginficant to mention since the beds are essensially flat (less than 10 degree dip) there was no tilt correction required and therefore the titt-corrected coordinates are not included in Table 4.

Most samples are characterized by a low coercitivty component that is removed in the first four AF steps (2.5 mT – 10 mT). This component is randomly directed which is typical of a unstable magnetizations carried by multidomian magnetite. These "soft" components hold no geological significance and are often the result of drilling and sample preparation. Apart from this component, samples from Hartley Hill quarry generally show two to three distinct demagnetization components (see Fig. 12). These are labled A, B, and C, and are discussed below.

Samples from Pramberg (HCB) and O'Donehough (HCC) did not show within site reproducibility, and these samples were generally dominated by randomly directed single linear trends towards the origin. These components may be the result of poor magnetic carriers or due to lightning. The Pramberg quartz porphyry location would have allowed for a fold test, but due to the poor reproducibility the test could not be obtained. The results from these two sites are not further discussed.

4.2.1.1 Component A (AF, Low coercivity)

As mentioned, the first couple of demagnetization steps for most samples define random low coercivity and low stability components. Their removal is followed by the unblocking of component A (between ~7.5 and 20 mT) as northerly and upward directed linear

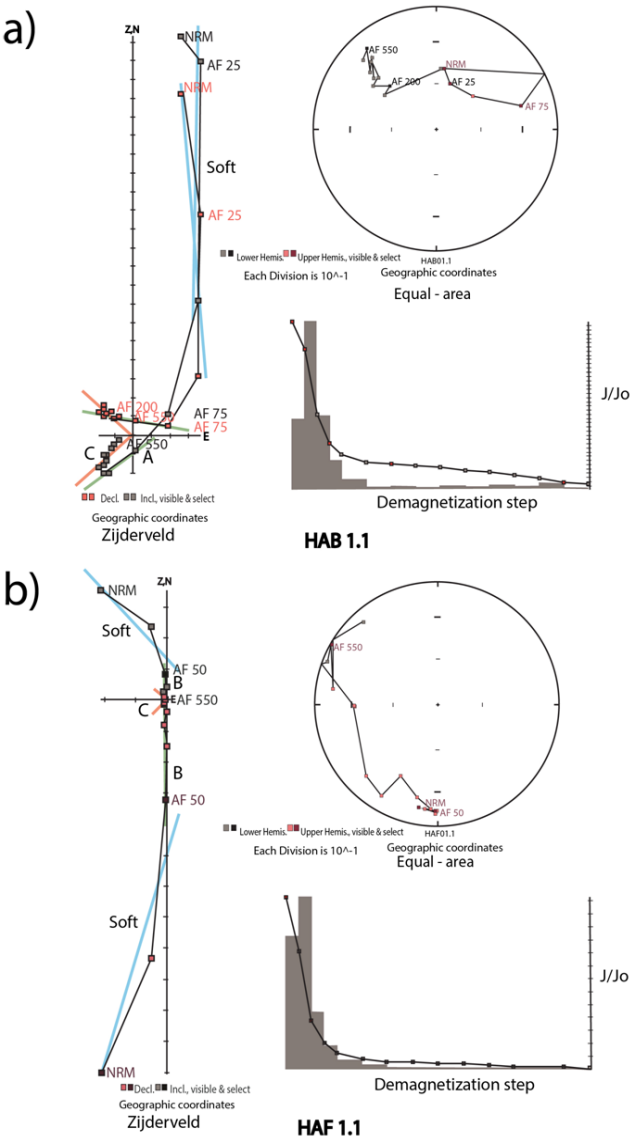

Fig. 12. Demagnetization behavior of representative samples on Zijderveld diagrams, equal-area plots and as J/Jo diagrams. Zijderveld plots display magnetic vector endpoints projected back onto the horizontal surface (red symbols), as well as the N-S vertical surface (grey symbols). On equal-area nets the same vector endpoints are shown (upper hemisphere = red symbols and lower hemisphere = grey symbols). The J/Jo plots show the progressive demagnetization of the magnetization (J) with successive demagnetization steps. a) Sample HAA displays three magnetic componentes. The first (indicated in blue) is a "soft" component, and it is followed by northerly and upward directed component A (green) and the high stability component C in red. b) Sample HAF also displays three magnetic componentes. The first (indicated in blue) is a "soft" component, and it is followed by shallow and southerly directed component B (green) and the high stability component C in red.

Table 4. The Fisher statistical revision of the least-squares (after Kirschvnik, 1980).

Component A (Low coercivity)

Location	*Site*	*n/N*	*L/C*	*Declination*	*Inclination*	*α95*	*κ*
Hartley Hill quarry	HAA	9/16	7/0	332.4	-52.2	7.4	48.9
	HAB	10/15	11/0	50.2	-63.8	9.8	25.2
	HAC	9/11	11/0	15.6	-64.3	17.2	9.9
	HAD	4/5	4/0	43.0	-65.4	40.36	4.16
	HAE	12/14	9/0	348.4	-80.0	16.0	8.4
	HAF	5/14	-	40.9	-28.3	21.6	13.5
	HAG	4/14	8/0	18.5	-43.5	18.5	25.6
	HLO4*	3/4	3/0	346.4	-46.9	37.4	7.9

Component B (Moderate coercivity)

Location	*Site*	*n/N*	*L/C*	*Declination*	*Inclination*	*α95*	*κ*
Hartley Hill quarry	HAA	-	-	-	-	-	-
	HAB	-	-	-	-	-	-
	HAC	-	-	-	-	-	-
	HAD	-	-	-	-	-	-
	HAE	-	-	-	-	-	-
	HAF	7/7	7/0	199.7	-16.8	9.8	39.2
	HAG	-	-	-	-	-	-
	HAH	8/12	-	154.3	7.8	30.5	4.3
Moshaneng dolerites	JP11**	10/5	5/0	180.5	-28.1	5.8	69.2

Component C (High coercivity)

Location	*Site*	*n/N*	*L/C*	*Declination*	*Inclination*	*α95*	*κ*
Hartley Hill quarry	HAA	8/16	8/0	289.1	26.6	13.0	19.2
	HAB	8/15	8/0	304.9	36.9	14.1	16.3
	HAC	3/11	3/0	322.8	50.6	18.6	30.1
	HAD	3/5	3/0	291.2	34.6	15.5	42.6
	HAE	5/14	5/0	310.9	25.1	43.7	4.0
	HAF	4/14	4/0	306.4	38.0	23.4	12.3
	HAG	4/14	4/0	312.2	44.1	22.7	17.3
	HAH	2/12	2/0	302.7	37.0		
	HLO4	4/4	4/0	275.7	-15.2	21.9	13.9
Moshaneng dolerites	JP9**	14/0		324.1	7.2	6.3	40.2
	JP10**	13/1		315.0	0.9	7.5	31.6

α95 = 95% circle of confidence
Meaningless data has been specified with red color.
* The HLO4 was sampled by Evans et al. (2002).
** The JP9, JP10 and JP11 were sampled by Hanson et al. (2004).

segments. The A components are near parallel to the present dipole field of the Earth at the sampled localities. But it should be noted there there is a large spread in site means (Fig. 13), suggesting partial overlap with either lower or higher stability components.

4.2.1.2 Component B (Moderate coercivity)

After the removal of component A an different component of intermediate coercivity unblock in samples from two sites (i.e., two samples from site HAA, all the samples site HAF and HAH). These components are shallow and to the south (Fig. 14). This component, referred to as the component B, is generally poorly constrained (in one case with a MAD angle >15).

4.2.1.3 Component C (High coercivity)

The high coercivity samples display high resistence to

the demagnetization prosedure and are generally removed between 35 – 100 mT steps. These were removed as origin-seeking linear trends or stable endpoints of demagnetization and are referred to as component C. The component C means from various sites concentrates in the northwestern hemisphere of the equal area projection and exhibits a positive, moderate to shallow inclination (Fig. 15). Component C from site HLO4 of Evans et al. (2002) is distinct from the other sites, and might be adversely affected by the incomplete removal of lower stability components. It is not included in the subsequent site mean calculation.

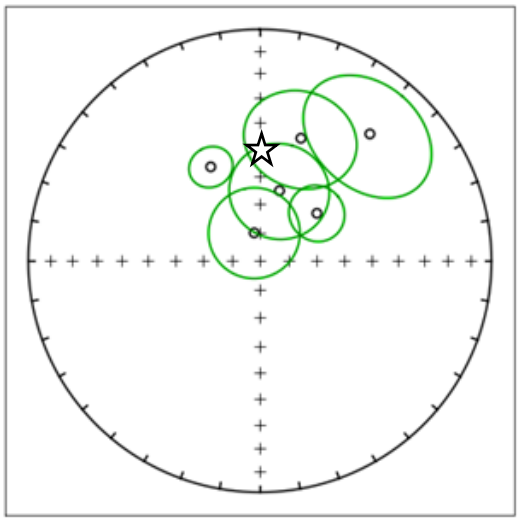

Fig. 13. Component A site means (in geographic coordinates) compared to the position of the present day axial dipole field at the sampling locality (represented by the star). Site mean values with α95 > 25° are not shown.

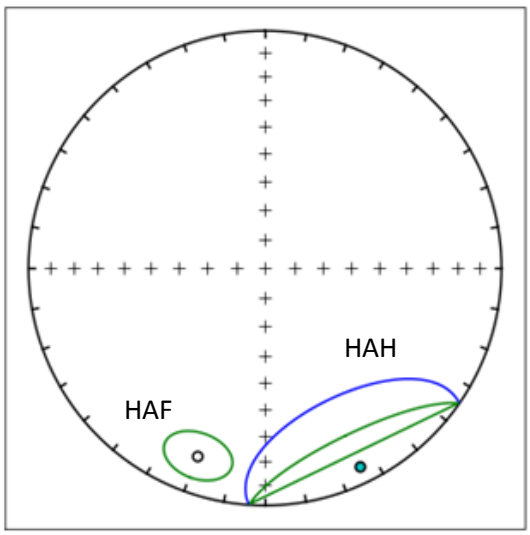

Fig. 14. Component B site means (in geographic coordinates). The two samples from site HAA are not shown.

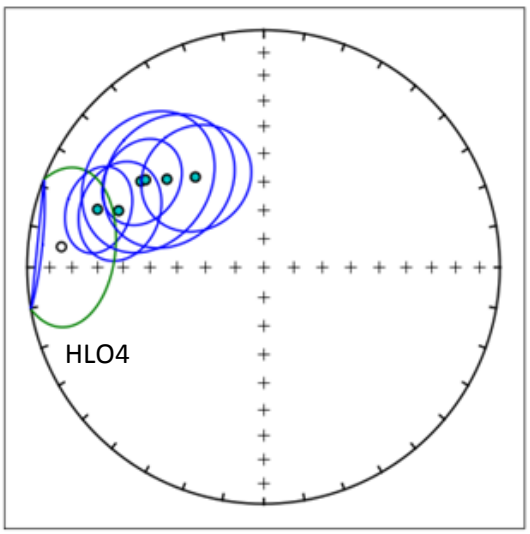

Fig. 15. Component C site means (in geographic coordinates). Site mean values with α95 > 25° are not shown. The mean from HLO4 is a clear outlier.

5 Discussion

5.1 Interpretation of the Paleomagnetic data and paleopole calculation

5.1.1 Characteristics of low coercivity components

Component A is removed below 25 mT and is near parallel to the Earth's present axial dipole field. This component is interpreted as either a recent viscous remanent magnetization or a chemical remanent magnetization recorded during recent weathering.

Component B is only recorded in two flow units (HAF and HAH) and in two of samples from site HAA. This component is shallow and southerly directed. It is interesting to note flow unit HAF in which component B is best developed was noticeably foliated with an apple green mineral (presumably epidote) along foliation planes. The foliation was trending NW-SE and was dipping moderately to steep. The NW-SE trend of the foliation is similar to that of ~1.2 – 1.0 Ga regional deformation increasingly affecting rocks further to the west. There is a good possibility that component B developed in association with the regional deformation that occurred during the Namaqua-Natal orogeny in the Mesoproterozoic.

5.1.2 The characteristics of the high coercivity component

Component C has high coercivity and it is removed during AF demagnetization between 35 – 100 mT. It is directed westnorth westerly and downwards at a moderate to shallow angle. It is the only component

that displays reproducibility and consistency throughout the demagnitization process and it is recognizeable in the majority of the sampled units. Given its high stability and consistency it is interpreted as the primary magnetic direction.

Component C was present in all of the sampled units at Hartley Hill, but it became progressiely deteriorated defined towards the top of the quarry. In sites HLO4, HAF and HAG it was present in about 30 – 50 % of samples and α95 values ranged from 21.9 to 23.4. These sites were still included in the mean calculation. Typically in paleomagnetic studies α95 ≤ 16° is used as a cutoff, but a higher cutoff seems justified in this case given the general "noisy" behavior of samples. The component was very poorly defined in site HAE (α95 = 43.7 and k = 4.0) and at site HAH component C was only identified in two samples. These two sites are not included in mean calculation.

5.1.3 Calculating the paleomagnetic pole

According to Tauxe (2007): "A paleomagnetic pole is defined as an average of a number of VGPs sufficient to average out secular variation or in other words the mapping of an average of a number of paleomagnetic directions to the equivalent pole". Calculation of the paleomagnatic pole demands the assumption of an axial-dipol geomagnetic field and a stable earth radius throughout the geological time and equal to the earth's present day radius. A pole position calculated for the direction of a geomagnetic field at one location and at a single point in time, is refered to as "Virtual geomagnetic pole" or VGP to be short (Butler, 1998).

A VGP was calculated for component B from site HAF at 48.8˚N and 53.2˚E (dp=5.2, dm=10.1). When compared to paleopoles from the Kaapvaal craton this VGP is very similar to the 1.2 – 1.1 Ga section of the Mesoproterozoic apparent polar wander path (APWP, see Fig. 16). This confirms the suspicion that this component is related to the regional deformation of the Namaqua-Natal orogeny.

To be able to calculate the paleomagnatic pole for the Hartley Basalt Formation, the VGPs of the sampled sites in this study was combined with the VGPs for the two sites of the similarly aged Moshaneng Doleriite (sites JP9 and JP10 of Hanson et al. 2004b). The calculated VGPs for the primary component in each site are presented in Table 5 and illustrated in Figure 17a. The combination of eight VGPs yield a paleomagnetic pole at 22.7°N, 328.6°E, A95 = 11.7 and k = 23.4.

5.1.4 Reliability of the paleomagnetic pole

Evans et al. (2002) calculated the paleomagnetic pole for Hartley Basalt formation by combining all the data from various sampling sites into vectors and line fits, to decide various components, and treated the eight lava flows as one site. This approach produced a pole with less accuracy. In this study, we initially calculated a virtual geographic pole (VGP) for each sampled unit, treating each site individually, and then combined all the site's VGPs to calculate a paleomagnetic pole. This approach is more statistically accurate. The pole of this study is a clear improvement on that of Evans et al. (2002).

Van der Voo (1990) proposed seven criteria Q-scale for assessing the reliability of a paleopole. A reliable pole might not necesserily meet all of the 7 criteria to define a 'key pole', but the more points criteria a pole meets, the more reliable it becomes. Van der Voo's seven criteria for assessing the reliability of a paleopole:

1. Accurate geochronological age of the formation (presuming that the geochronological age is

Table 5. Calculated VGPs for the primary component in each site based on the tilt-corrected direction (achieved by the combined data).

Calculated VGP's				
Location	*Site*	*VGP Latitude*	*VGP Longitude*	*α95(°)*
Hartley Hill quarry	HAA	9.6	314.4	13.0
	HAB	18.0	329.0	14.1
	HAC	21.0	349.2	18.6
	HAD	8.6	319.8	15.5
	HAE*	27.2	327.0	43.7
	HAF*	18.6	330.5	23.4
	HAG*	19.3	337.9	22.7
	HAH*	16.4	327.6	-
	HLO4*	6.9	287.7	21.9
Moshaneng dolerites	JP9	45.0	329.4	6.3
	JP10	39.6	318.5	7.5
	JP11	50.2	26.0	5.8

* The samples that are excluded from pole calculation.

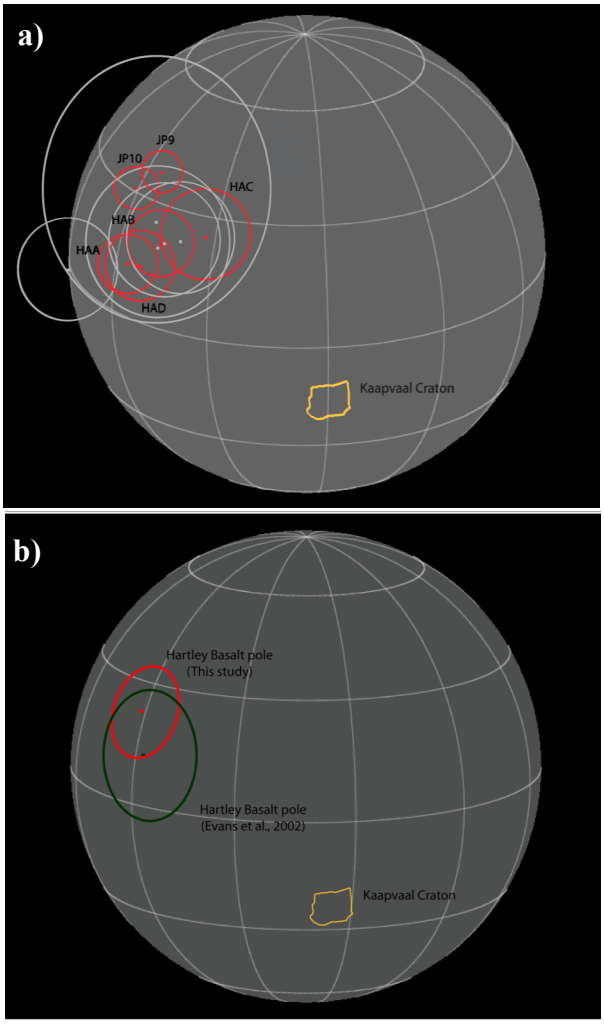

Fig. 16. a) Position of the VGPs calculated for components C in accordance with Table 5. The VGPs that are shown in red were used in pole calculation while the grey VGPs were not included. b) Comparison of the Hartley Basalt pole calculated by Evans et al., 2002 (Green) vs the pole calculated in this study (Red).

about the same as the magnetization age).
2. Having suffcient amount of samples (N > 24, k ≥ 10, α95 ≤ 16.0).
3. Structural control and tectonic coherence with the craton or the block involved.
4. Performing field tests that constrain the age of magnetization (fold, conglomerate, contact…).
5. Decent demagnetization procedure that facilitates the subtraction of vectors.
6. The existence of reversals.
7. No suspecion of remagnetization (clear difference with the younger age paleopoles).

The paleomagnetic pole of Evans et al. (2002) at 12.5°N, 332.8°E, κ =18.6, α95 = 16.0 fails to fullfil a number of these criteria: 1.) sufficient amount of sites (fewer than 24), 2.) lack of field tests and reversals tests and 3) similarity to younger poles (Early Cambrian according to Evans et al.,1998), and therefore rates as a 3 on the van der Voo (1990) reliability scale.

The Hartley Basalt paleopole, calculated in this study, rates a 4 on the Q-scale of reliability from van der Voo (1990), failing to fullfil sufficient amount of sites, field tests and the presence of a reversal. But given the significan increase in the number of samples per site and the statistically more valid pole calculation, the new Hartley Pole is considered a significant improvement on that of Evans et al. (2002). Figure 16 display the new Hartley Basalt Pole (this study) versus other paleoproterozoic to mesoproterozoic poles.

5.1.5 Paleoproterozoic-Mesoproterozoic Apparent Polar Wander

The Hartley Basalt pole calculated in this study can be further used in completion of the Paleoproterozoic apparent polar wander path (APWP) for Kaapvaal Craton. In this study we compare the Paleoproterozic APWP with the Meosproterozoic APWP and include three recent poles, 1840 – 1870 Ma Black Hills Swarm (Lubnina et al., 2010), 1108 – 1112 Ma Umkondo lavas (Gose et al., 2006) and the Hartley Basalt pole calculated in this study. As it is shown in Figure 18, the path of the Paleoproterozoic APWP starts with 2.22 Ga Ongeluk lava (Cornell et al., 1996) and continues northwesterly till about 2.0 Ga. From ~2.0 Ga the path carries on southwesterly till ~1.9 Ga. At ~1.9 Ga the polar wander displays a previously discovered loop northwards (De Kock et al., 2006) which is further confirmed by the Hartley Basalt (HAR) pole in this study. From ~1.9 Ga to ~1.87 Ga the path moves towards a more south easterly direction. The Mesoproterozoic polar wander path shows a west to southwesterly direction. Component B (low coercivity) plots in close vicinity of the Mesoproterozoic poles which can be an indicator of an overprint. The poles that are used for comparison in Figure 17 are mentioned in Table 6.

5.2 ~1.9 Ga magnetism of Kaapvaal and Zimbabwe cratons

A critical question is whether the rocks of 1.93 – 1.92 and 1.88 – 1.84 Ga belong to a common regional-scale event or represent two separate events, which in the case the latter is correct, these rocks are unrelated. This question has critical bearings on the timing of formation of Kalahari Craton, i.e. the timing of collision between the Kaapvaal and Zimbabwe craton, because:

1. Paleomagnetic measurements of mafic rocks that provide spatial information at a certain time relies on accurate age determinations.
2. Recognition of magmatic events can be arranged in so called “barcodes”. Comparisons of barcodes will provide information whether or

not crustal blocks were adjacent relative to each other ("next neighbours") or widely dispersed.

3. Recognition of discrete, potentially unrelated, events are necessary for identifying the location of igneous centres, and potentially, the mechanisms of emplacement (e.g. intra-crustal rifting or mantle plume).

Indeed, current geochronological data suggest that mafic units in Kaapvaal and Zimbabwe can be divided into two separate events at 1.93 – 1.92 and 1.88 – 1.84 Ga, below summarized.

5.2.1 ~1.9 Ga igneous rocks in Kaapvaal and Zimbabwe

The Tsineng Dyke Swarm and the Hartley Basalt Formation: The 1928 ± 4 Ma age obtained for the Hartley Basalt formation (Cornell, 1998) falls within the error range of the 1922 ± 6 Ma age for the RP353 dyke in this study. The most recent U-Pb zircon dating of the Hartley Basalt formation was done by Da Silva (2011), yielding 1920.5 ± 4.1 Ma (from Mooihoek locality in north of Olifantshoek) and 1931 ± 20 Ma (from interbedded Quartzite in Boegoebergdam lava). These new datings (1920.5 ± 4.1 – 1931 ± 20 Ma) are also in line with the dating of the RP353 dyke (this study) and can possibly confirm the relation between the Tsineng Dyke Swarm and the Hartley Basalt formation.

Geochronology and vicinity of these igneous rocks hence suggest that the ENE-trending Tsineng dyke swarm and the Hartley Basalt formation originated from the same magma. Considering the trend, spread and the fanning shape of the Tsineng dyke swarm (Fig. 18) indicate a link to a mantle plume or a mag-

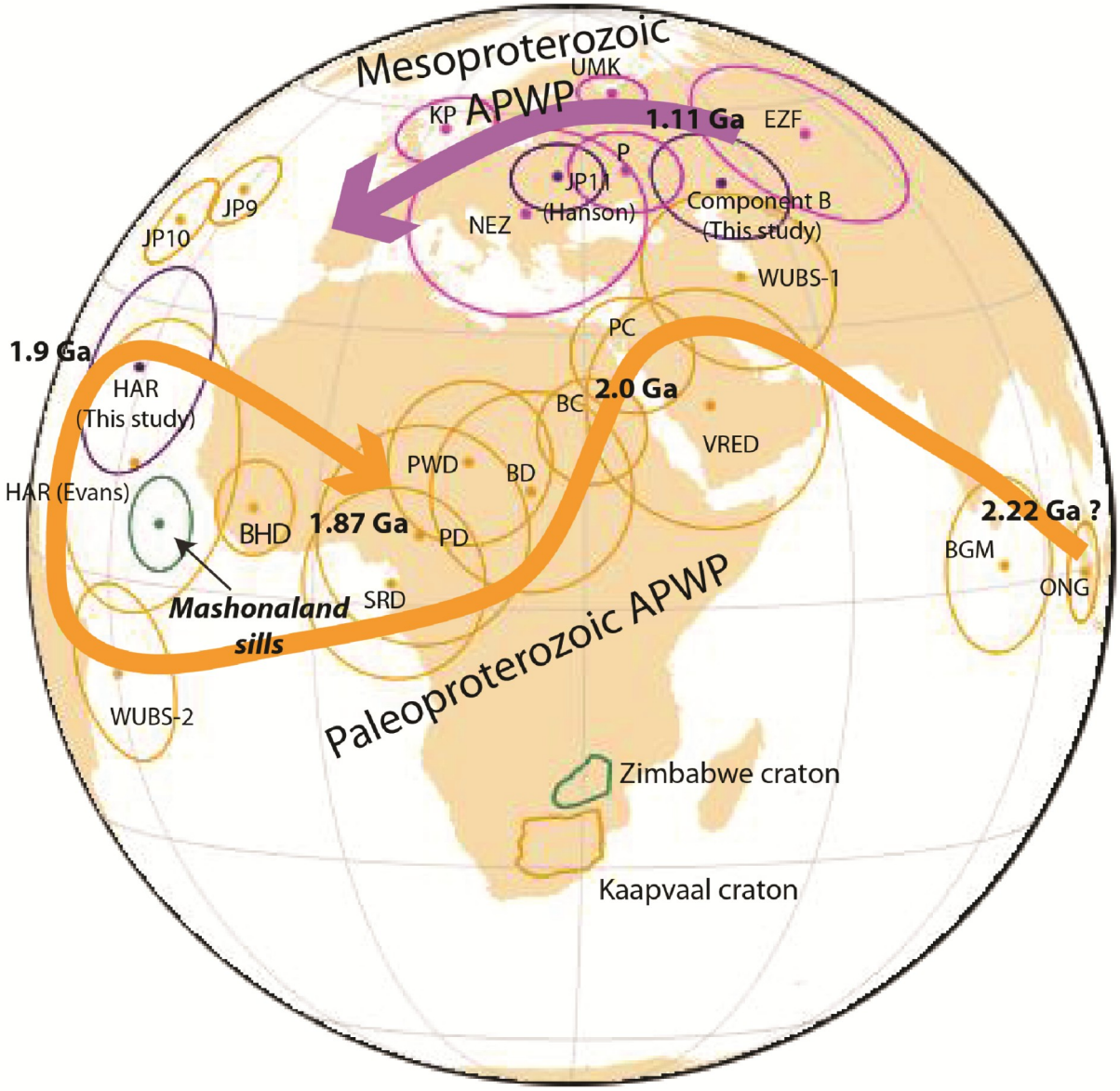

Fig. 17. Comparison of the selected paleopoles from paleoproterozic to lower Jurassic in Kaapvaal and Zimbabwe cratons. Outline of the continents and the Kaapvaal craton are shown for reference. The detailed information of each pole is mentioned *in Table 6*.

Table 6. The Early Paleoproterozoic to Early Jurassic Poles from the Kaapvaal–Kalahari Craton.

Rock unit	Code	Age (Ma)	Age ref.	N	Latitute, °N	Longtitude, °E	K	dp, deg	dm, deg	Pmag ref.
Ongeluk lava	ONG	2222 ± 13	1	22	-00.5	100.7	38.3	5.3	5.3	2
Basal Gamagara/ Mapedi	BGM	2060–2200	3	32	02.2	081.9	–	7.2	11.5	4
Phalaborwa 1	PB1	2060.5 ± 0.6	5	11	35.9	044.8	–	6.9	10.5	6
Bushveld Complex	BC	2050 ± 12	7		19.2	30.8		5.8		8
Vredefort Impact	VRED	2023 ± 4.0	9, 10,11	–	21.8	44.5	–	11.3	15.4	12
Limpopo metamorfic "A"	LMA	1950–1980?	13	21	26.1	022.3	–	7.9	10.3	13
Hartley Basalt formation	HAR	1928 ± 4	14	7	42.1	356.1	7.3	–	22.0	15
Moshaneng dolerites	MD	~1927	16		42.3	323.95			6.9	16
Sand river Dykes	SRD	1876 ± 68?	13	6	02.3	009.1	–	10.3	10.3	13
Post-Waterberg Sills	PWD	1874.6 ± 3.9	16		15.6	17.1	–	–	8.9	16
Phalaborwa dykes	PBD		7		7.6	12.1			11.8	7
Soutpansberg sills	SS	~1830	17		32.9	24.4		13.3	19.0	18
Black Hills dyke swarm	BHDS	1840–1870	19		09.4	352.0		4.3	5.8	20
Mashonaland sills	MASH	1830 ± 230	21,22	29	07.6	338.2	28.3	5.1	5.1	23,24
Namaqua-Natal	NN	~1050	25		8.0	328.0		20	15.0	
Ntimbankulu Granite	NG	~1050			27.0	327.0			18.0	
Umkondo lavas	UL	1112–1108	18		63.4	16.4			13.7	18
Karoo dykes	KD	183 ± 2	27		-68.3	93.7		7.0	7.0	27

References: (1) Cornell et al., 1996; (2) Evans et al., 1997; (3) Beukes et al., 2002; (4) Evans et al., 2002; (5) Reischmann, 1995; (6) Morgan and Briden, 1981; (7) Letts et al., (unpublished) (8) Letts et al., 2009; (9) Kamo et al., 1996; (10) Hargraves, 1970; (11) Hart et al., 1995; (12) Carporzen 2006; (13) Morgan, 1985; (14) Cornell et al., 1998; (15) This study; (16) Hanson et al., (2004b); (17) Barton, 1979; (18) Gose et al., (2006); (19) Olsson et al., 2012; (20) Lubnina et al., 2010; (21) Söderlund et al., 2010; (22) Compston and McElhinny, 1975; (23) McElhinny and Opdyke, 1964; (24) Bates and Jones, 1996; (25) Onstott et al., 1986; (26) ?; (27) Hargraves et al., 1997.

matic center that was located close to the western border of the Kaapvaal craton (black star in Fig. 18). Plume centers and Large igneous provinces (LIPs in short) are often associated with each other. Despite the fact that shape and distribution of the dykes of the Tsineng swarm indicate a mantle plume origin it is difficult to estimate the exact magnitude of this magmatic event due to erosion and lack of geochronology. In order to come to a definite conclusion, a more thorough investigation is needed for identifying additional 1.93 – 1.92 Ga units in both Kaapvaal and possibly Zimbabwe Craton.

Post-Waterberg intrusions (Moshaneng dolerites): The Waterberg Group comprises of a succession of Proterozoic sediments deposited on the Archean to Paleoproterozoic rocks of Kaapvaal Craton. Mafic intrusions are dominated by doleritic sills and several irregular mafic bodies and dykes, intrusive into sediments of the Waterberg Group (successive Proterozoic deposits at the northern part of Bushveld complex) and underlying rocks (Hanson et al., 2004) (Fig. 18). Hanson et al. (2004) sampled three sites within Moshaneng dolerites (part of the Moshaneng complex, located in the southeastern part of Botswana) and yielded robust U-Pb baddeleyite ages of 1927.1 ± 0.7, 1927.3 ± 0.7 and 1927.7 ± 0.5 Ma for this suit (Hanson et al., 2004). These ages are coeval with the ca. 1928 Ma Hartley Basalt Formation and considering the similar geochemistry of both units these may belong to the same event.

Post-Waterberg sills: Ca. 1.88 Ga intrusions within the Waterberg are represented by sills of the Waterberg Group in the northern Kaapvaal. Three intrusions yielded precise U-Pb baddeleyite ages of 1878.8 ± 0.5, 1873.7 ± 0.8 and 1871.9 ± 1.2 Ma (Hanson et al., 2004).

The Black Hills swarm: The NE-NNE trending Black Hills swarm is located northeast of the Bushveld Complex (Fig. 18). The swarm is made up of mainly ca. 2.7 Ga dykes as well as a younger set of dykes with tholeiitic composition. Olsson et al. (2012) obtained precise U-Pb baddeleyite ages ranging from ca. 1862 to ca. 1839 Ma for the younger generation of these dykes. The 1.86 – 1.84 dykes of the Black Hills

swarm also differ from the ~2.7 Ga dykes in seemingly having a NNE trend and many dykes seem to continue into the Transvaal basin (Fig. 18). For example one of the NEE-trending dykes near Lydenburg area dates back to approximately 1.88 Ga (Olsson, unpublished data).

Soutpansberg sills and lavas: The Soutpansberg Group is located in the northern part of the Limpopo Province (Fig. 18). This group consists of basaltic lavas, sedimentary rocks (syn-rift sequence) and layers of pink massive quartzite, deposited after an erosional period (post-rift sequence). According to Cheney et al. (1990), the base of this group unconformably overlies ca. 1957 Ga granites, representing a reliable lower age for the Soutopansberg group. Rb-Sr isochron dates obtained from samples of basaltic flow yield ca. 1750 Ma (Barton, 1979). Compared with the post-Waterberg dolerites, higher concentration of REE elements in Soutpansberg sills and other geochemical differences yet suggest that the post-Waterberg Group has originated from a petrologically different magma during approximately the same time at which the Soutpansberg sills and lavas were formed (Hanson et al, 2004). In this context, it must be recognized that the age of Soutpansberg sills and lavas are poorly dated. The strongest argument for that these mafic units are 1.88 – 1.84 Ga in age is their location just north of the 1.88 – 1.84 Ga Black Hills swarm, however a recent paper by Geng et al. (2014) attained the youngest reliable ages for the Soutpansberg sills 1831 ± 15 Ma and 1832 ± 9 Ma representing the early magmatic phase of volcanism, and concluded that deposition of the Soutpansberg volcano-sedimentary succession started around 1830 Ma (Fig. 18).

Mashonaland sills: The Mashonaland sills are of continental tholeiictic composition (Stubbs et al., 1999) intruding the basal Archean deposits (granites and greenstone belts). Sills are concentrated in north east of Zimbabwe Craton (Fig. 18) although some occur also further south. U-Pb baddeleyite datings of three sills gave 1.88 to 1.87 Ga (Söderlund et al., 2010, Hanson et al., 2011).

Mazowe dyke swarm: The E-trending Mazowe dyke swarm is associated with the Mashonaland sills at the northeast of Zimbabwe Craton. Although a precise dating on this swarm has still not been performed, Rb-Sr whole rock dating yielded 1870 ± 600 Ma (Compston and McElhinny, 1975) for this unit. The 1.88 Ga age obtained by Söderlund et al. (2010) for the Mashonaland sills and its similarity in paleomagnetic direction to the Mazowe river dykes indicate the Mazowe dyke swarm and the Mashonaland sills belong a common event at ca. 1.88 Ga.

5.2.2 Recognition and evidences for two discrete igneous events at 1.93 – 1.92 Ga and a 1.88 – 1.84 Ga.

Current geochronological data of mafic rocks on Kaapvaal and Zimbabwe strongly suggest two discrete events of magmatic activity, rather than a single protracted event of magmatism. The 1.93 – 1.92 Ga event is defined by the Tsineng dyke swarm (including the RP353 dyke within this swarm), Hartley Basalt formation, post-Waterberg sills (Moshaneng dolerites), whereas the 1.88 – 1.84 Ga mafic rocks generation comprises the Waterberg sills, Soutpansberg volcanics, the Mashonaland sills and NE-SW to NNE-SSW trending Black Hill dykes. These subgroups are shown in black and violet respectively in Figure 18.

In contrast to the 1.93 – 1.92 Ga event which seems unique for Kaapvaal, the 1.88-1.84 Ga event can be identified in both Kaapvaal and Zimbabwe cratons. Earlier studies such as Wilson et al. (1990) and Kamber et al. (1995) stated that the 1.88 Ga Mashonaland sills were intruded in response to strike-slip movements along Limpopo and Magondi Belts and that the deformation of Magondi Belt coincides with the Mashonaland Igneous Event (Carnpbell et al., l99l). Also it had been assumed that based on similar paleomagnetic signatures the E-trending Mazowe River (Wilson et al., 1987) and the Sebanga dykes were the feeders of the Mashonaland sills (Jones et al., 1975; Mushayandebvu et al., 1995b; Bates and Jones, 1996). However, U-Pb baddeleyite dating of the Sebanga Port dyke (2408.3 ± 2.0 obtained by Söderlund et al., 2010) has proved that theory wrong. By considering the trend of the Mazowe River dykes in northern Zimbabwe and also the extent of Mashonaland Igneous Event it is plausible that an igneous center at the north east of Zimbabwe was responsible for the intrusion of Mashonaland sills and Mazowe River dykes, as proposed by Klausen et al., 2010. As shown in Figure 18, the location of this magmatic center is far from the center proposed in this study for the 1.93 – 1.92 Tsineng swarm and Hartley Basalt formation. Another possible magnetic center can be placed at the east of Limpopo Belt in relations with post-Waterberg sills, the NNE-NE trending dykes of the Black Hills swarm and possibly even parts of the Soutpansberg sills (Fig. 18).

Olsson et al., 2012 raised an interesting question regarding a possible link between the NE-NEE-trending dykes of the Black Hills swarm and the Tsineng dyke swarm. However, the new age (1922 ± 6 Ma) for the RP353 dyke of the Tsineng swarm obtained in this study, indicates a clear age difference between the two swarms. In addition, as shown in Figure 18, there's a slight difference in trend between the ~1.88 Ga Black Hills dykes (marked with the grey dashed lines) and the NE-trending Tsineng dykes. If extrapolating the trend of ~1.88 Ga Black Hills dykes towards the western margin of the Kaapvaal Craton, they would continue far south of the Tsineng dykes. This observation justifies the conclusion that the Tsineng swarm and the Black Hills swarm are not related and cannot have originated from same magmatic sources. Moreover, Lubnina et al. (2010) obtained a paleomagnetic pole for the NE-trending dykes of the Black Hills swarm and by plotting this pole it is obvious that the Black Hills swarm's paleopole does

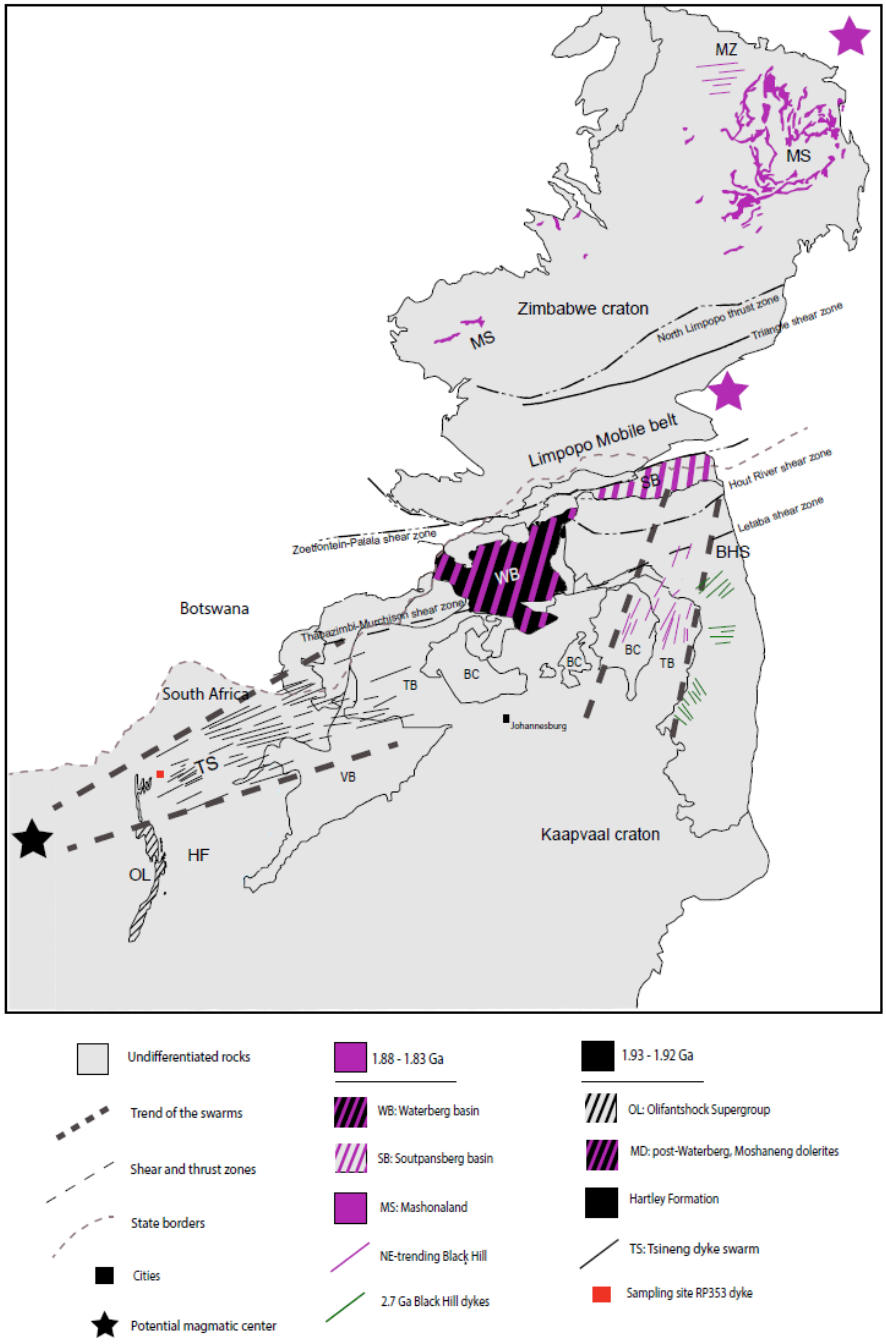

Fig. 18. Map showing the location of 1.93 – 1.92 Ga and 1.8 – 1.84 Ga magmatic rocks in Kaapvaal and Zimbabwe cratons. The location of proposed magmatic centers for the ~1.92 Ga (black star) and ~1.88 Ga (violet stars) igneous events are tentatively marked.

not overlap with the paleopole for the Hartley Basalt Formation (this study, Fig. 19). This observation indicates that the Kaapvaal Craton was located in different positions and moved approximately to more southerly latitudes from ~1.92 Ga to ~1.88 Ga (Fig. 18). Distinct differences in age, geographic distribution and geochemistry between the Tsineng dyke swarm and the NE-trending dykes of the Black Hills swarm robustly show that these two swarms are unrelated.

Additional support for two discrete events at 1.93 – 1.92 Ga and 1.88 – 1.84 Ga stem from geochemistry. According to Cornell et al. (1998), the Hartley Basalt formation has a tholeiitic composition with high total Fe content (around 16 %), constant Na_2O levels and low K_2O levels. The basalts show a slight negative Eu anomaly and have positive εSr and negative εNd values, indicator of a relative enrichment in LREE elements. It also has relatively high Rb/Sr ratio in comparison with the chondric mantle. Considering the geochemical characteristics of Hartley basalt and its low μ_2 value (Cornell, 1998), it can be concluded that this formation originated from a source depleted in U,

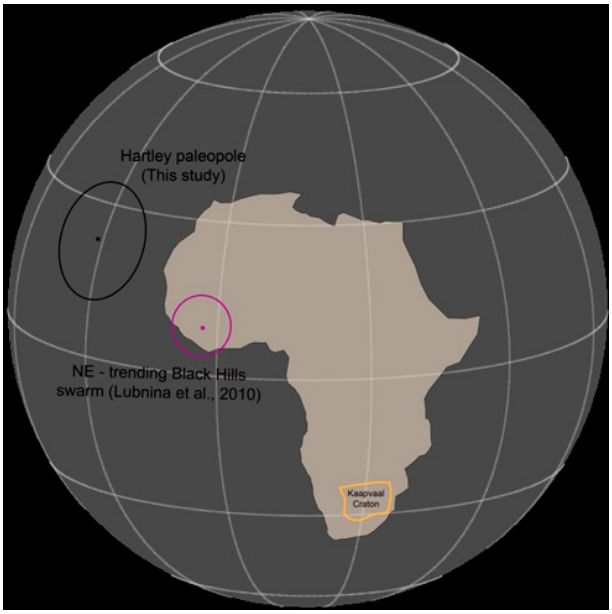

Fig. 19. Comparison of the ~1.92 Ga Hartley Basalt's paleopole (this study) with ~1.86 – 1.84 Ga NE-trending Black hills swarm's paleopole (Lubnina et al., 2010).

possible the lower crust.

The Hartley Basalt formation, Moshaneng dolerites and ~1.88 post-Waterberg dolerites all have a sub-alkali basaltic and, in some rare cases, andesitic composition (MgO values of ~9 – 4.5 w% and Fe-enrichment). However, as shown in Figure 20, there are several geochemical differences between the 1.93 – 1.92 Ga and 1.88 – 1.84 Ga units. Fe content in Hartley Basalt and Moshaneng dolerites is much higher than all the ~1.88 Ga sills in Kaapvaal. Ti, V and Y concentrations are also higher that the younger unit. In contrast Al concentration in ~1.92 Ga units are lower than ~1.88 Ga units. Although some petrographical similarities between ~1.92 Ga and ~1.88 Ga rocks, resemblance in the major-element geochemistry and the degree of deuteric alteration has been recognized in recent studies (Hanson et al., 2004), the ratio of REE and incompatible trace elements differs between the rocks of the two events.

5.3 Timing of the formation of Kalahari Craton

The term Kalahari Craton was first proposed by Clifford in 1970 for designation of the Precambrian shield of South Africa. For decades, the collision between Kaapvaal and Zimbabwe cratons at the Limpopo Belt and the subsequent formation of Kalahari Craton has been the subject of extensive debates (e.g. Zeh et al., 2004; Söderlund 2010; Hansen et al 2011). Some earlier studies such as McCourt and Armstrong (1998) have associated this collision to a low-pressure granulite facies metamorphism at the Central Zone of Limpopo Belt dated at 2.6 – 2.7 Ga (Watkeys, 1984;

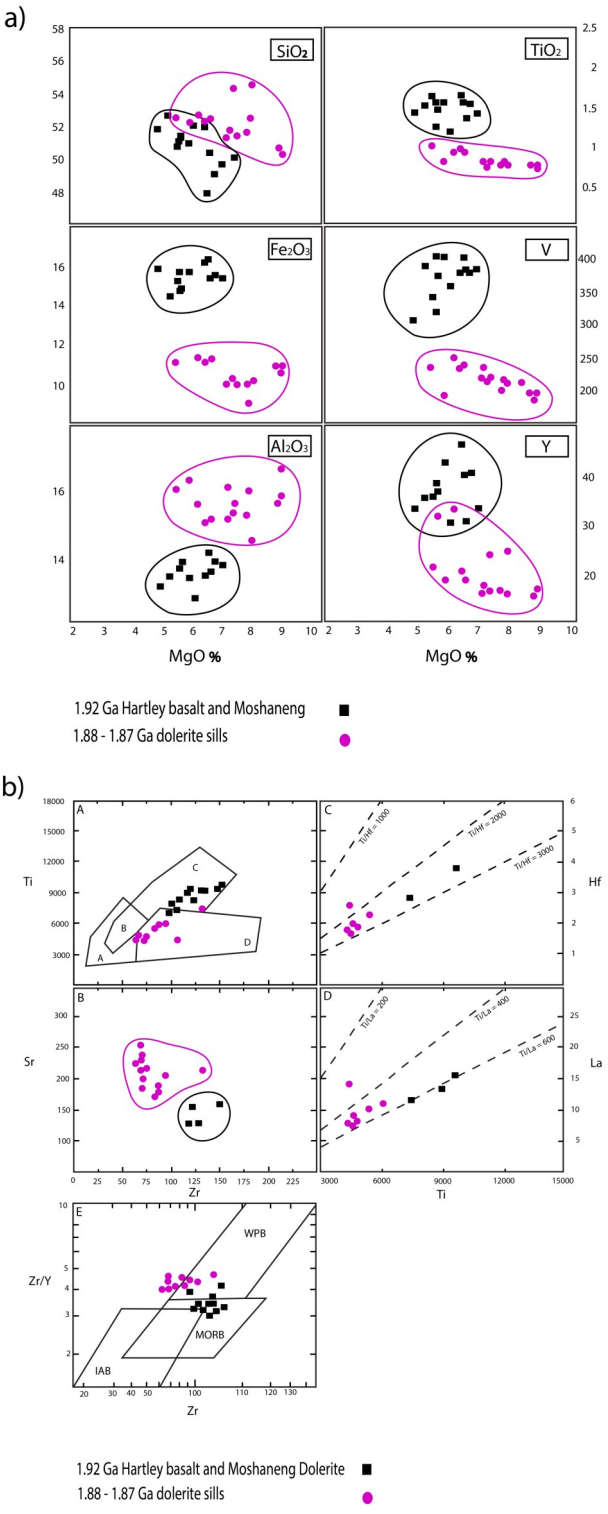

Fig. 20. a) A selection of major and trace elements plotted vs MgO for the Hartley Basalt (Cornell et al., 1998), Moshaneng dolerites, ~1.88 to ~1.87 Ga post-Waterberg dolerite sills (Ward, 2002; Bullen, unpublished data). Major oxides in weight %, trace elements in ppm. b): Incompatible elements variation diagrams for the Hartley Basalt (Cornell et al., 1998), Moshaneng dolerites, ~1.88 to ~1.87 Ga post-Waterberg dolerite sills (Ward, 2002; Bullen, unpublished data (Modified after Hanson et al., 2004b).

Holzer et al., 1998; Zeh et al., 2004). However, the discovery of a younger event of ~2.0 – 1.9 Ga metamorphism in the Central Zone of the belt through various geochronological methods (Kröner et al., 1999);Buick et al. 2006) constrained the timing of collision between the two cratons and the formation of Kalahari Craton to ~2.0 Ga. Other studies by Kramers et al. (2006) and Van Reenen et al. (2008), have also put the timing of the collision at around 2.0 Ga referring to an event of high-grade metamorphism and ductile shearing in the Central Zone of the Limpopo belt. This metamorphic event has the hall marks of an isothermal decompression comprised of a primary crustal thickening followed by uplift, resulted from the collision between Kaapvaal and Zimbabwe cratons (Holzer et al., 1998). Collision at ca. 2.0 Ga was also inferred by Söderlund et al. (2010) based on "barcode matching", i.e comparing the timing of emplacement of mafic igneous suites from Kaapvaal and Zimbabwe cratons. Nevertheless, the timing of formation of Kalahari is still debated.

To further complicate the situation, Hanson et al. (2011) noticed a 39° distance between the Mashonaland paleopole and the paleopole for post-Waterberg diabases and Soutpansberg sills and lavas (pole WSD in Hanson et al., 2011). This would require that Kaapvaal and Zimbabwe cratons were as far as 2000 km apart at around 1.88 Ga, hence proposing that the two cratons amalgamated in post-1.88 times (Hanson et al., 2011).

Notably, the paleomagnetic data of Hansen et al. (2011) were not tilt-corrected. In order to calculate the distance between two paleopoles one has to consider the primary angle and direction of each unit (here post-Waterberg and Mashonaland sills). The post-Waterberg sills intrude into a sedimentary basin, thus their orientation (horizontal) was controlled by the sedimentary bedding of their host rocks. However, the same cannot be performed for the Mashonalad sills since they are intruded into granitic bedrock. It is therefore possible that the current strike of the Mashonaland sills is not primary

Another argument against a 2000 km displacement after 1.88 Ga is to take a look at other ~1.88 Ga paleopoles of Kaapvaal Craton such as the pole for the NE-trending dykes of the Black Hills swarm (NBH, Lubnina et al., 2010). As shown in the Figure 21, the NBH pole plots in close vicinity of the Mashonaland pole (MASH, Bates and Jones, 1996). The reason why the two poles do not completely overlap can be that the NBH pole represents a VGP obtained from a single NE-trending dyke of the Black Hills swarm. Separate VGPs for one specific time can differ by 15° due to paleocircular variations hence the NBH pole does not signify the average of all the ~1.88 Ga dykes of this swarm. If a new paleopole can be obtained by sampling a number of these NE-trending dykes the result will probably overlap with the Mashonaland pole. Also the geochronological and the paleomagnetism data for the Black Hills swarm have not been obtained from the same dyke or dykes. Attaining the paleomagnetic directions for certain dykes in this swarm that have been dated (Olsson et al., 2011) might resolve the lack of an overlap.

Another problem with Hanson et al. (2011) pole calculation is that the paleomagnetic data for the post-Waterberg sills and the Soutpansberg sills have opposite polarities. Also according to recent datings by Geng et al. (2014), the latter is in some parts much younger (ca. 1830 Ma) than post-Waterberg intrusions ranging from 1.88 to 1.86 Ga. The combination of the younger Soutpansberg sills data with the post-Waterberg data to achieve a single paleopole (WSD) is not a reasonable choice and can affect the reliability of this pole.

Another efficient tool to correlate and match different magmatic events and pin point the timing of the collision between Kaapvaal and Zimbabwe cratons are barcode diagrams. Today with the use of LIP barcode records for the each craton, it is possible to achieve an independent time frame for the formation of the Kalahari Craton. Matching barcodes indicate that crustal blocks were in close vicinity at the time of magmatic events whereas absence of common barcodes indicates crustal blocks were located far apart. The geochronological result obtained in this study together with the earlier geocronological findings for both ~1.92 Ga and ~1.88 Ga units can be applied to the completion of the barcode diagrams for Kaapvaal and Zimbabwe cratons (Fig 22).

In this study, the barcode diagrams illustrate the occurrence of coeval magmatic events in both Kaapvaal and Zimbabwe cratons at ca. 1.88 Ga (Hanson et al., 2004b and Söderlund et al, 2010), ca. 1.1 Ga (Hanson et al., 2004a) and ca. 0.18 Ga (Jourdan et al., 2006);

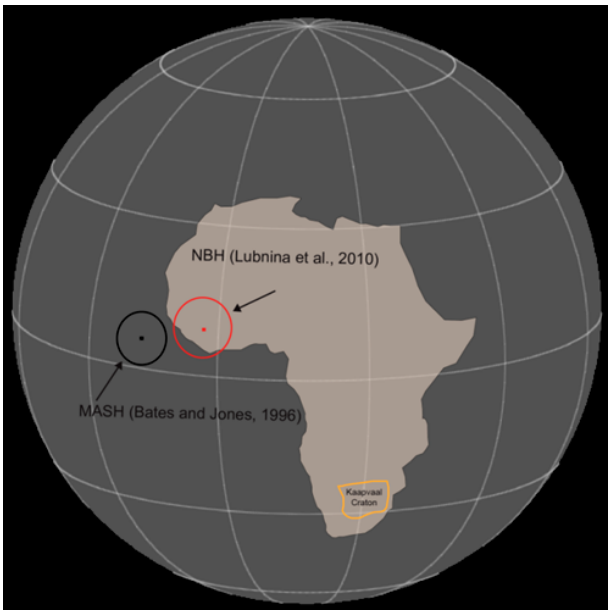

Fig. 21. Comparison of the palopoles for the Mashonaland sills in Zimbabwe Craton (MASH, Bates and Jones, 1996) and the NE-trending dykes of the Black Hills swarm in Kaapvaal Craton (NBH, Lubnina et al., 2010).

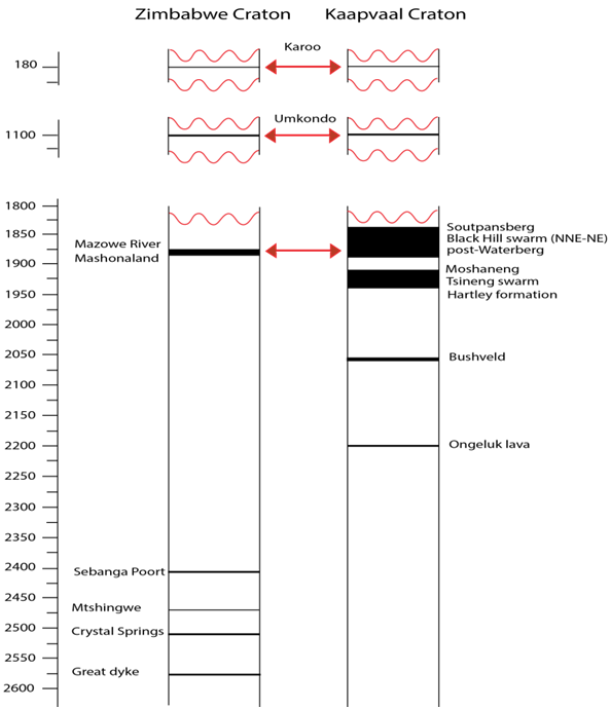

Fig. 22. Barcode record of Neo-Archaean till Neo-Proterozoic Kaapvaal and Zimbabwe craton. The arrows illustrates possible age match between mafic intrusions such as radiating dyke swarms, sill provinces and other components of LIP.

among which the ca 1.88 Ga provides the oldest minimum age for the formation of the Kalahari Craton. The U–Pb baddeleyite emplacement ages of ca. 1.88 Ga for a number of NE-trending dykes of the Black Hills swarm (Olsson et al., 2012) confirms this minimum age. Considering the absence of the Great Dyke (2.57 Ga) and Sebanga dyke ages (2.51 Ga, 2.47 Ga and 2.41 Ga) in the Kaapvaal Craton and in correspondence the absence of magmatism at ca. 2.06 Ga (the formation of the Bushveld complex) in the Zimbabwe Craton strongly suggests that the two cratons were apart during the early Paleoproterozoic (Söderlund et al. 2010). The primary clastic depositions in the Waterberg basin and the orogeny in the Limpopo Belt at ~2.0 Ga (Cheney and Twist, 1986; Hanson et al., 2004a,b) agree with collision at ca. 2.0 Ga (Söderlund et al. 2010).

In the end, the 1.93-1.92 Ga generation of sills and dykes in Kaapvaal has not yet been reported anywhere in Zimbabwe Craton, whereas the 1.88 Ga magmatism is evident on both Kaapvaal and Zimbabwe cratons (see Fig. 21). The fact that the 1.93 – 1.92 Ga magmatic event appears to be unique for the Kaapvaal Craton could indicate that collision occurred sometime within ca. 1.93 to 1.88 Ga.

6 Conclusions

- Baddeleyite U-Pb dating of the RP353 dyke of the Tsineng dyke swarm at the western margin of the Kaapvaal Craton yields a robust and concordant age of 1922 ± 6 Ma for this mafic unit. This age establishes a direct temporal link between the RP353 doleritic unit and the Hartley Basalt formation (1928 ± 4 Ma, Cornell, 1987) of the Olifantshoek Supergroup and the Moshaneng dolerites, and potentially other coeval units not yet discovered.

- The Tsineng dyke swarm and the NE-trending dykes of the Black Hills swarm belong to separate and unrelated magmatic events. The trend, spread and the fanning shape of the Tsineng dyke swarm points towards a magmatic center located close to the western border of the Kaapvaal Craton, whereas the proposed magmatic centerfor the NE-treding dykes of the Black Hills swarm is here proposed to have been located at the north east of the Limpopo Belt. Clear difference in geochronology, lack of overlap between the two paleopoles and a clear difference in trends of the ~1.88 Ga Black Hills dykes with the NE-trending Tsineng dykes support the two swarms are unrelated.

- The primary direction in this study (component C) yields a paleomagnetic pole at N°= 22.7, E°=328.6, α95=11.7, which rates 4 (out of 7) in the proposed reliability scale by Van der Voo (1990).

- The the 2000 km displacement theory by Hanson et al., 2011 is questioned given the fact that the lack of a required tilt correction for the Mashonalad sills due to possible rotations after their intrusion in a granitic basin, can lead to inaccuracy in paleomagnetic calculations and interpretations.

- Paleomagnetic evidence (closeness of ~1.88 Ga poles in Kaapvaal and Zimbabwe cratons) together with barcode diagrams (based on the geochronological data from the two cratons) indicate the amalgamation of Kaapvaal and Zimbabwe cratons and the subsequent formation of Kalahari Craton happened sometime between ca.1.92 to ca.1.88 Ga.

7 Acknowledgements

I am extremely grateful for being presented with the opportunity to work on this great project. I would like to thank my two wonderful supervisors, Ulf Söderlund

and Michiel de Kock, for supporting me tirelessly throughout this thesis and guiding me every step of the way. Thanks to Ashley Gumsley for his help during the field work in South Aftica and reviewing parts of my thesis. Thanks to Robert Fuchs and Mimmi Nilsson for their great help in baddeleyite separation and TIMS analysis. I would like to acknowledge the staff of the Department of Geology at the University of Johannesburg for their welcome and hospitality. Great thanks to Fisnik Balija for his immense help with editing and preparing this thesis. In the end, I would like to greatly thank my family for their unconditional support and encouragement.

8 References

Barton, J.M., 1979. The chemical compositions, Rb–Sr isotopic systematics and tec-tonic setting of certain post-kinematic mafic igneous rocks, Limpopo MobileBelt, southern Africa. Precambrian Res. 9, 57–80.

Barton, E.S., Altermann, W., Williams, 1.S.& Smith, C.B., 1994.U-Pb zircon age for a tuff in the Camp bell Group, Griqnaland West Sequence, South Africa: implications for early Proterozoic rock accumulation rates. Geology, 22: 343-346.

Barton Jr., J.M., Holzer, L., Kamber, B., Doig, R., Kramers, J.D. & Nyfeler, D., 1994. Discrete meta morphic events in the Limpopo belt, southern Africa: Implications the application of P-T paths in complex metamorphic terrains. Geology 22, 1035-1038. Doi:10.1130/00917613(1994)022<103 5:DMEITL> 2.3.CO;2.

Barton, J. & Pretorius, W., 1997. The lower unconformity-bounded sequences of the Sout pansberg Group and its correlatives remnants of a Proterozoic large igneous province. South African Journal of Geology 100, 335-339.

Bates, M.P. & Jones, D.L., 1996. A palaeomagnetic investigation of the Mashonaland dolerites, north-east Zimbabwe. Geophys. J. Int. 126, 513–524.

Beukes, N.J., Gutzmer, J., 1996. A volcanic-exhalative origin for the world's largest (Kalahari) manganese field: A discussion of the paper by D.H. Cornell and S.S. Schtitte: Mineralium Deposita, v. 31, p. 242-245.

Beukes, N. J., H. Dorland, J. Gutzmer, M. Nedachi, and H. Ohmoto, Tropical laterites, life on land, and the history of atmospheric oxygen in the Paleopro terozoic, Geology, 30, 491–494, 2002.

Brandl, G., Cloete, M., Anhaeusser, C.R., 2006. Archean Greenstone Belts. In Johnson, M.R., Anhaeusser, C.R., Thomas, R.J. (Eds.), The Geology of South Africa. Geological Society of South Africa, Johannesburg, pp. 9-56.

Buick, I.S., Hermann. J., Williams, I.S., Gibson, R.L. & Rubatto, D., 2006. A SHRIMP U-Pb and LA-ICP-MS trace element study of the petrogensis of garnet-cordierite-orthoamphibole gneisses from the Central Zone of the Limpopo Belt, South Africa. Lithos 88, 150-172.

Cheney, E. S. and Twist, D., 1986. The Waterberg "Basin" - a reappraisal. Transactions of the Geological Society of South Africa, 89, 353-360.

Cheney, E. S., J. M. Barton Jr., and G. Brandl., 1990. Extent and age of the Soutpansberg sequences of southern Africa, S. Afr. J. Geol., 93, 664 – 675.

Cornell, D.H., 1987. Stratigraphy and petrography of the Hartley Basalt Formation, northern Cape Province. South African Journal of Geology 90 (1), 7-24.

Cornell, D.H., Schütte, S.S. & Eglington, B.L., 1996. The Ongeluk basaltic andesite formation in Griqualand West, South Africa: submarine alterna tion in a 2222 Ma Proterozoic sea. Precambrian Research 79, 101-123.

Cornell, D.H., Armstrong, R.A & Walraven, F., 1998. Geochronology of the Hartley Formation, South Africa: constraints on the Kheis tectogenesis and the Kaapvaal Craton's earliest Wilson cycle. Jounal of African Earth Sciences, vol. 26, No. 1, 5-27.

De Kock, M.O., Evans, D.A.D., Dorland, H.C., Beukes, N.J. & Gutzmer, J., 2006. Paleomagnetism of the lower two unconformity-bounded sequences of the Waterberg Group, South Africa: Towards a better defined apparent polar wander path for the Paleoproterozoic Kaapvaaal Craton. South African Journal of Geology, vol. 109, No. 1-2, 157-182.

Dorland, H.C., 2009. PhD thesis, University of Johannesburg, Johannesburg, South Africa, 310 pp.

Eglington, B.M. & Armstrong, R.A., 2004. The Kaapvaal Craton and adjacent orogens, South Africa: a geochronological database and overview of the geological development of the craton. South African Journal of Geology, vol. 107, No. 1-2, 13-32.

Ernst, R.E., Buchan, K.L., 2001. The use of mafic dike swarms in identifying and locating mantle plumes. In: Ernst, R.E., Buchan, K.L. (Eds.), Mantle Plumes: Their Identification Through Time. Geol.

Soc. America Spec. Paper 352, pp. 247–265.

Evans, D. A. D., Gutzmer, J., Beukes, N. J. and Kirschvink, J. L. (2001). Paleomagnetic constraints on ages of mineralization in the Kalahari Manganese Field, South Africa. Economic Geology, 96, 621-631.

Evans, D.A.D., Beukes, N.J. & Kirschvink, J.L., 2002. Palaeomagnetism of a lateritic paleoweathering horizon and overlying Paleoproterozoic red beds from South Africa: Implications for the Kaapvaal apparent polar wander path and a confirmation of atmospheric oxygen enrichment. Journal of Geophysical Research 107. Doi:10.1029/2001JB000432.

Geng, H., Brandl, G., Sun, M., Wong, J. & Kröner, A., 2014. Zircon ages defining deposition of the Palaeoproterozoic Soutspansberg Group and further evidence for Eoarchaean crust in South Africa. Precambrian Research 249, 247-262.

Goldberg, A.S., 2010. Dyke swarms as indicators of major extensional events in the 1.9-1.2 Ga Columbia supercontinent. Journal of Geodynamics 50, p. 176-190.

Gose, W.A., Hanson, R.E., Dalziel, I.W.D., Pancake, J.A., & Seidel, E.K., 2006, Paleomagnetism of the 1.1 Ga Umkondo large igneous province in southern Africa. Journal of Geophysical Research, vol. 111, B09101, p. 1–18. Doi:10.1029/2005JB003897.

Griffin, W.L., O'Reilly, S.Y., Natapov, L.M. & Ryan, C.G., 2003. The evolution of lithospheric mantle beneath the Kalahari Craton and its margins. Lithos 71, 215- 241.

Hanson, R.E., Gose, W.A., Crowley, J., Ramezani, S.A., Bowring, D.S., Hall, R.P., Pancake, J.A. & Mukwakwami, J., 2004. Paleoproterozoic intraplate magmatism and basin development on the Kaapvaal Craton: age, paleomagnetism and geochemistry of ~1.92 to ~1.87 Ga post-Waterberg dolerites. South African Journal of Geology 107, 233-254.

Hanson, R.E., Rioux, M, Gose, W.A., Blackburn, T.J., Bowring, D.S., Mukwakwami, J.& Jones, D.L., 2011. Paleomagnetic and geochronological evidence for large-scale post-1.88 Ga displacement between the Zimbabwe and Kaapvaal cratons along the Limpopo belt. Geology 39, 487-490. Doi: 10.1130/G31698.1.

Holzer, L., Barton, J.M., Paya, P.K. & Kramers, J.D., 1998. Tectonothermal history of the western part of the Limpopo Belt: tectonic models and new perspectives. Journal of African Earth Sciiences, vol. 28, No. 2, 383–402.

Hunter, D.R., 1974. Crustal development in the Kaapvaal craton. II. The proterozoic. Precambrian Research 1, 295-326.

Jacobs, J., Pisarevsky, S., Thomas, R.J. & Becker, T., 2008. The Kalahari Craton during the assembly and dispersal of Rodinia. Precambrian Research 160, 142-158.

Jaffey, A.H., Flynn, K.F., Glendenin, L.E., Bentley, W.C., Essling, A.M., 1971. Precision measurement of half-lives and specific activities of 235U and 238U. Physical Review, vol. 4, p. 1889-1906.

James, D.E., Niu, F. & Rokosky, J., 2003. Crustal structure of the Kaapvaal craton and its significance for early crustal evolution. Lithos 71, 413– 429.

Kamber, B.S., Kramers, J.D., Napier, R., Cliff, R.A., Rollinson, H.R., 1995. The Triangle Shearzone, Zimbabwe, revisited: new data document an important event at 2.0 Ga in the Limpopo Belt. Precambrian Res. 70, 191–213.

Kirschvink, J.L., 1980. The least-squares line and plane and the analysis of plaeomagnetic data. Geophyical Journal of Royal astronomical Society 62, 699-718.

Klausen, M.B., Söderlund, U., Olsson, J.R., Ernst, R.E., Armoogam, M., Mkhize, S.W. & Petzer, G., 2010. Petrological discrimination among Precambrian dyke swarms: Eastern Kaapvaal craton (South Africa). Precambrian Research 183, 501-522.

Kröner, A., Jaeckel, P., Brandl, G., Nemchin, A.A. & Pidgeon, R.T., 1999. Single zircon ages for granotoid gneisses in the Central Zone of the Limpopo Belt, Southern Africa and geodynamic significance. Precambrian Research 93, 299-337.

Letts, S., Torsvik, T.H., Webb, S.J. & Ashwal, L.D., 2009. Palaeomagnetism of the 2054 Ma Bushveld Complex (South Africa): implications for emplacement and cooling. Geophysical Journal International 179, 850-872. Doi: 10.1111/j.1365-246X.2009.04346.x

Letts, S., Torsvik, T.H., Webb, S.J. & Ashwal, L.D., 2010. New Palaeoproterozoic palaeomagnetic data from the Kaapvaal Craton, South Africa. Geological Society , London, Special Publications 357, 9-26.

Lubninaa, N., Ernst R., Klausen M. & Söderlund U., 2010. Paleomagnetic study of Neoarchean-

Paleoproterozoic dykes in the Kaapvaal Craton. Precambrian Research 183, 523–552.

Ludwig, K.R., 2003. Isoplot 3.00: A geochronological toolkit for Microsoft Excel. Berkeley Geochronology Center Special Publication 2003, 1-70.

Mushayandebvu, M.F., Bates, M.P. & Jones, D.L., 1995. Anisotropy of magnetic susceptibility results from the Mashonaland dolerite sills and dykes of northeast Zimbabwe. Physics and Chemistry of Dykes, Baer & Helmann (eds), Balkerna, Rotter dam, 151-161.

Olsson, J.R., Söderlund, U., Klausen, M.B & Ernst, R.E., 2010. U-Pb baddeleyite ages linking major Archean dyke swarms to volcanic-rift forming events in the Kaapvaal craton (South Africa), and precise age for the Bushveld Complex. Precambrian Research 183, 490-500.

Olsson, J.R., Söderlund, U, Hamilton, M.A., Klausen, M.B., Helfrrich, G.R., 2011. A late Archean radiation dyke swarm as possible clue to the origin of the Bushveld Complex. Nature Geoscience, vol. 4, 865-869. Doi: 10.1038/NGEO-1308.

Olsson, J.R., 2012. U-Pb baddeleyite geochronology of Precambrian mafic dyke swarms and complexes in southern Africa – regional scale extensional events and the origin of the Bushveld Complex

Stubbs, H.M., Hall, R.P., Hughes, D.J. & Nesbitt, R.W., 1999. Evidence for a high Mg andesitic parental magma to the East and West satellite dykes of the Great Dyke, Zimbabwe: a comparison with the continental tholeiitic Mashonaland sills. Journal of African Earth Sciences, vol. 28, No. 2, 326-336.

Söderlund, U. & Johansson, L., 2002. A simple way to extract baddeleyite (ZrO2). Geochemistry Geophysics Geosystems 3, 1014, doi: 10.1029/2001GC0-00212.

Söderlund, U., Hofmann, A., Klausen, M.B., Olsson, J.R., Ernst, R.E. & Persson, P.-E., 2010. Towards a complete magmatic barcode for the Zimbabwe craton: Baddeleyite U–Pb dating of regional dolerite dyke swarms and sill complexes. Precambrian Research 183, 388-398.

Tauxe, L., Butler, R.F., Van der Voo, R., Banerjee, S.K., 2010. Essentials of paleomagnetism. University of California Press, Berkeley.

Van der Voo, R., 1990. The reliability of paleomagnetic data. Tectonophysics 184, 1-9.

Van Reenen, D.D., Boshoff, R., Smit, C.A., Perchuk, L.L., Kramers, J.D., McCourt, S. & Armstrong, R.A., 2008. Geochronological problems related to polymetamorphism in the Limpopo Complex, South Africa. Gondwana Research 14, 644-662.

Wilson, J.F., 1990. A craton and its cracks: some of the behaviour of the Zimbabwe block from the Late Archaean to the Mesozoic in response to horizontal movements, and the significance of some of its mafic dyke fracture patterns. Journal of African Earth Sciences, vol. 10, No. 3, 483-501.

Zeh, A., Klemd, R., Buhlmann, S. & Barton, J.M., 2004. Pro- and retrograde P-T evolution of granulites of the Beit Bridge Complex (Limpopo Belt, South Africa): constraints from quantitive phase diagrams and geotectonic implications. Journal of metamorphic Geology 22, 79-95. Doi:10.1111/j.1525-1314.2004.00501.x

Tidigare skrifter i serien ”Examensarbeten i Geologi vid Lunds universitet”:

366. Karlsson, Michelle, 2013: En MIFO fas 1-inventering av förorenade områden: Kvarnar med kvicksilverbetning Jönköpings län. (15 hp)
367. Michalchuk, Stephen P., 2013: The Säm fold structure: characterization of folding and metamorphism in a part of the eclogite-granulite region, Sveconorwegian orogen. (45 hp)
368. Praszkier, Aron, 2013: First evidence of Late Cretaceous decapod crustaceans from Åsen, southern Sweden. (15 hp)
369. Alexson, Johanna, 2013: Artificial groundwater recharge – is it possible in Mozambique? (15 hp)
370. Ehlorsson, Ludvig, 2013: Hydrogeologisk kartering av grundvattenmagasinet Åsumsfältet, Sjöbo. (15 hp)
371. Santsalo, Liina, 2013: The Jurassic extinction events and its relation to CO_2 levels in the atmosphere: a case study on Early Jurassic fossil leaves. (15 hp)
372. Svantesson, Fredrik, 2013: Alunskiffern i Östergötland – utbredning, mäktigheter, stratigrafi och egenskaper. (15 hp)
373. Iqbal, Faisal Javed, 2013: Paleoecology and sedimentology of the Upper Cretaceous (Campanian), marine strata at Åsen, Kristianstad Basin, Southern Sweden, Scania. (45 hp)
374. Kristinsdóttir, Bára Dröfn, 2013: U-Pb, O and Lu-Hf isotope ratios of detrital zircon from Ghana, West-African Craton – Formation of juvenile, Palaeoproterozoic crust. (45 hp)
375. Grenholm, Mikael, 2014: The Birimian event in the Baoulé Mossi domain (West African Craton) — regional and global context. (45 hp)
376. Hafnadóttir, Marín Ósk, 2014: Understanding igneous processes through zircon trace element systematics: prospects and pitfalls. (45 hp)
377. Jönsson, Cecilia A. M., 2014: Geophysical ground surveys of the Matchless Amphibolite Belt in Namibia. (45 hp)
378. Åkesson, Sofia, 2014: Skjutbanors påverkan på mark och miljö. (15 hp)
379. Härling, Jesper, 2014: Food partitioning and dietary habits of mosasaurs (Reptilia, Mosasauridae) from the Campanian (Upper Cretaceous) of the Kristianstad Basin, southern Sweden. (45 hp)
380. Kristensson, Johan, 2014: Ordovicium i Fågelsångskärnan-2, Skåne – stratigrafi och faciesvariationer. (15 hp)
381. Höglund, Ida, 2014: Hiatus - Sveriges första sällskapsspel i sedimentologi. (15 hp)
382. Malmer, Edit, 2014: Vulkanism - en fara för vår hälsa? (15 hp)
383. Stamsnijder, Joaen, 2014: Bestämning av kvartshalt i sandprov - metodutveckling med OSL-, SEM– och EDS-analys. (15 hp)
384. Helmfrid, Annelie, 2014: Konceptuell modell över spridningsvägar för glasbruksföroreningar i Rejmyre samhälle. (15 hp)
385. Adolfsson, Max, 2014: Visualizing the volcanic history of the Kaapvaal Craton using ArcGIS. (15 hp)
386. Hajny, Casandra, 2014: Ett mystiskt ryggradsdjursfossil från Åsen och dess koppling till den skånska, krittida ryggradsdjursfaunan. (15 hp)
387. Ekström, Elin, 2014: – Geologins betydelse för geotekniker i Skåne. (15 hp)
388. Thuresson, Emma, 2014: Systematisk sammanställning av större geoenergianläggningar i Sverige. (15 hp)
389. Redmo, Malin, 2014: Paleontologiska och impaktrelaterade studier av ett anomalt lerlager i Schweiz. (15 hp)
390. Artursson, Christopher, 2014: Comparison of radionuclide-based solar reconstructions and sunspot observations the last 2000 years. (15 hp)
391. Svahn, Fredrika, 2014: Traces of impact in crystalline rock – A summary of processes and products of shock metamorphism in crystalline rock with focus on planar deformation features in feldspars. (15 hp)
392. Järvin, Sara, 2014: Studie av faktorer som påverkar skredutbredningen vid Norsälven, Värmland. (15 hp)
393. Åberg, Gisela, 2014: Stratigrafin i Hanöbukten under senaste glaciationen: en studie av borrkärnor från IODP’s expedition nr 347. (15 hp)
394. Westlund, Kristian, 2014: Geomorphological evidence for an ongoing transgression on northwestern Svalbard. (15 hp)
395. Rooth, Richard, 2014: Uppföljning av utlastningsgrad vid Dannemora gruva; april 2012 - april 2014. (15 hp)
396. Persson, Daniel, 2014: Miljögeologisk undersökning av deponin vid Getabjär, Sölvesborg. (15 hp)
397. Jennerheim, Jessica, 2014: Undersökning av långsiktiga effekter på mark och grundvatten vid infiltration av lakvatten – fältundersökning

och utvärdering av förhållanden vid Kejsarkullens avfallsanläggning, Hultsfred. (15 hp)

398. Särman, Kim, 2014: Utvärdering av befintliga vattenskyddsområden i Sverige. (15 hp)
399. Tuvesson, Henrik, 2014: Från hav till land – en beskrivning av geologin i Skrylle. (15 hp)
400. Nilsson Brunlid, Anette, 2014: Paleoeko logisk och kemisk-fysikalisk undersökning av ett avvikande sedimentlager i Barsebäcks mosse, sydvästra Skåne, bil dat för ca 13 000 år sedan. (15 hp)
401. Falkenhaug, Jorunn, 2014: Vattnets kretslopp i området vid Lilla Klåveröd: ett kunskapsprojekt med vatten i fokus. (15 hp)
402. Heingård, Miriam, 2014: Long bone and vertebral microanatomy and osteo-histology of 'Platecarpus' ptychodon (Reptilia, Mosasauridae) – implications for marine adaptations. (15 hp)
403. Kall, Christoffer, 2014: Microscopic echinoderm remains from the Darriwilian (Middle Ordovician) of Västergötland, Sweden – faunal composition and applicability as environmental proxies. (15 hp)
404. Preis Bergdahl, Daniel, 2014: Geoenergi för växthusjordbruk – Möjlig anläggning av värme och kyla i Västskåne. (15 hp)
405. Jakobsson, Mikael, 2014: Geophysical characterization and petrographic analysis of cap and reservoir rocks within the Lund Sandstone in Kyrkheddinge. (15 hp)
406. Björnfors, Oliver, 2014: A comparison of size fractions in faunal assemblages of deep-water benthic foraminifera—A case study from the coast of SW-Africa.. (15 hp)
407. Rådman, Johan, 2014: U-Pb baddeleyite geochronology and geochemistry of the White Mfolozi Dyke Swarm: unravelling the complexities of 2.70-2.66 Ga dyke swarms on the eastern Kaapvaal Craton, South Africa. (45 hp)
408. Andersson, Monica, 2014: Drumliner vid moderna glaciärer — hur vanliga är de? (15 hp)
409. Olsenius, Björn, 2014: Vinderosion, sanddrift och markanvändning på Kristianstadsslätten. (15 hp)
410. Bokhari Friberg, Yasmin, 2014: Oxygen isotopes in corals and their use as proxies for El Niño. (15 hp)
411. Fullerton, Wayne, 2014: REE mineralisation and metasomatic alteration in the Olserum metasediments. (45 hp)
412. Mekhaldi, Florian, 2014: The cosmic-ray events around AD 775 and AD 993 - Assessing their causes and possible effects on climate. (45 hp)
413. Timms Eliasson, Isabelle, 2014: Is it possible to reconstruct local presence of pine on bogs during the Holocene based on pollen data? A study based on surface and stratigraphical samples from three bogs in southern Sweden. (45 hp)
414. Hjulström, Joakim., 2014: Bortforsling av kaxblandat vatten från borrningar via dagvattenledningar: Riskanalys, karaktärisering av kaxvatten och reningsmetoder. (45 hp)
415. Fredrich, Birgit, 2014: Metadolerites as quantitative P-T markers for Sveconorwegian metamorphism, SW Sweden. (45 hp)
416. Alebouyeh Semami, Farnaz, 2014: U-Pb geochronology of the Tsineng dyke swarm and paleomagnetism of the Hartley Basalt, South Africa – evidence for two separate magmatic events at 1.93-1.92 and 1.88-1.84 Ga in the Kalahari craton. (45 hp)

LUNDS UNIVERSITET

Geologiska institutionen

Lunds universitet